

See discussions, stats, and author profiles for this publication at: <https://www.researchgate.net/publication/221836937>

Identification of an Acyl-Enzyme Intermediate in a meta-Cleavage Product Hydrolase Reveals the Versatility of the Catalytic Triad

ARTICLE in JOURNAL OF THE AMERICAN CHEMICAL SOCIETY · MARCH 2012

Impact Factor: 12.11 · DOI: 10.1021/ja208544g · Source: PubMed

CITATIONS

14

READS

52

6 AUTHORS, INCLUDING:



[Geoff P Horsman](#)

Wilfrid Laurier University

27 PUBLICATIONS 613 CITATIONS

[SEE PROFILE](#)



[Leonard J Foster](#)

University of British Columbia - Vancouver

180 PUBLICATIONS 7,307 CITATIONS

[SEE PROFILE](#)

Identification of an Acyl-Enzyme Intermediate in a *meta*-Cleavage Product Hydrolase Reveals the Versatility of the Catalytic Triad

Antonio C. Ruzzini,^{†,‡} Subhangi Ghosh,^{§,‡} Geoff P. Horsman,^{†,⊥} Leonard J. Foster,[†] Jeffrey T. Bolin,^{*,§} and Lindsay D. Eltis^{*,†,||}

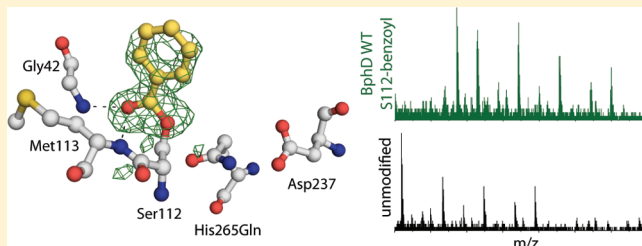
[†]Department of Biochemistry and Molecular Biology, University of British Columbia, Vancouver BC V6T 1Z3, Canada

[§]Purdue Cancer Research Center and Markey Center for Structural Biology, Department of Biological Sciences, Purdue University, West Lafayette, Indiana 47907, United States

^{||}Department of Microbiology and Immunology, University of British Columbia, Vancouver BC V6T 1Z3, Canada

S Supporting Information

ABSTRACT: *Meta*-cleavage product (MCP) hydrolases are members of the α/β -hydrolase superfamily that utilize a Ser-His-Asp triad to catalyze the hydrolysis of a C-C bond. BphD, the MCP hydrolase from the biphenyl degradation pathway, hydrolyzes 2-hydroxy-6-oxo-6-phenylhexa-2,4-dienoic acid (HOPDA) to 2-hydroxypenta-2,4-dienoic acid (HPD) and benzoate. A 1.6 Å resolution crystal structure of BphD H265Q incubated with HOPDA revealed that the enzyme's catalytic serine was benzoylated. The acyl-enzyme is stabilized by hydrogen bonding from the amide backbone of 'oxyanion hole' residues, consistent with formation of a tetrahedral oxyanion during nucleophilic attack by Ser112. Chemical quench and mass spectrometry studies substantiated the formation and decay of a Ser112-benzoyl species in wild-type BphD on a time scale consistent with turnover and incorporation of a single equivalent of ^{18}O into the benzoate produced during hydrolysis in H_2^{18}O . Rapid-scanning kinetic studies indicated that the catalytic histidine contributes to the rate of acylation by only an order of magnitude, but affects the rate of deacylation by over 5 orders of magnitude. The orange-colored catalytic intermediate, ES^{red}, previously detected in the wild-type enzyme and proposed herein to be a carbanion, was not observed during hydrolysis by H265Q. In the newly proposed mechanism, the carbanion abstracts a proton from Ser112, thereby completing tautomerization and generating a serinate for nucleophilic attack on the C6-carbonyl. Finally, quantification of an observed pre-steady-state kinetic burst suggests that BphD is a half-site reactive enzyme. While the updated catalytic mechanism shares features with the serine proteases, MCP hydrolase-specific chemistry highlights the versatility of the Ser-His-Asp triad.



INTRODUCTION

The α/β -hydrolase superfamily possesses one of the most widespread folds in nature and uses a conserved nucleophile–histidine–acid triad to catalyze a range of chemistries.¹ These enzymes also possess an 'oxyanion hole' and share a mirror image relationship with serine protease families' active site architecture, suggesting a conserved nucleophilic mechanism of catalysis.² Accordingly, covalent catalysis has been postulated in several α/β -hydrolases despite a lack of direct evidence.^{3–6} A notable exception is an acetyltransferase, DAC-AT, responsible for the last step in the biosynthesis of the β -lactam cephalosporin C, for which crystallographic data established the occurrence of an acyl-enzyme intermediate.⁷ Despite housing the necessary machinery to perform covalent catalysis, many α/β -hydrolases utilize a general base mechanism whereby the catalytic triad activates a small molecule, such as H_2O , H_2O_2 , or HCN.⁸ Family specific structural features, including various insertions and the orientation of active-site loops, contribute significantly to the catalytic mechanism of each α/β -hydrolase family.^{9,10}

The *meta*-cleavage product (MCP) hydrolases utilize a Ser-His-Asp triad to catalyze the hydrolysis of a C-C bond of a 2-hydroxy-6-oxo-dienoate formed by the dioxygenase-mediated *meta*-ring cleavage of catechols. Two of the most well-characterized MCP hydrolases are 2-hydroxy-6-oxo-nona-2,4-diene-1,9-dioic acid 5,6-hydrolase, MhpC, a dimeric enzyme from *Escherichia coli*, and 2-hydroxy-6-oxo-6-phenylhexa-2,4-dienoic acid (HOPDA) 5,6-hydrolase, BphD, a tetrameric enzyme from *Burkholderia xenovorans* LB400, whose catalytic triad is Ser112-His265-Asp237. In these enzymes, the active site lies between the α/β -hydrolase core and MCP hydrolase lid domains^{11,12} (Supporting Information Figure S1A). In BphD, the active site has polar (P-) and nonpolar (NP-) subsites that bind the MCP's dienoate and phenyl moieties, respectively. Five active site residues are conserved in MCP hydrolases but not other α/β -hydrolases: Arg190, Asn111, Phe175, Cys263, and Trp266 in BphD.¹³ Interestingly, all but Cys263 contact

Received: September 9, 2011

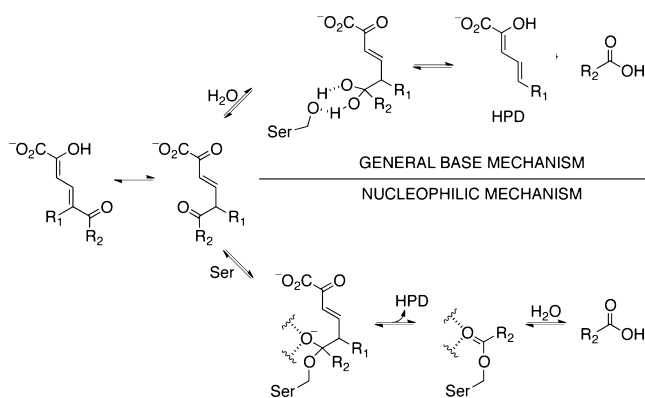
Published: February 17, 2012



the productively bound dioate,¹⁴ and substitution of any one of the five reduces the rate of C–C bond hydrolysis.¹³

The active site of MCP hydrolases reflects the difficulty of hydrolyzing a C–C bond compared to carbon–heteroatom bonds. Hydrolysis of the latter is typically facilitated by protonation of the leaving heteroatom to generate a positively charged electron sink. The MCP hydrolases cannot access such an electron sink as the leaving carbon cannot be protonated. Instead, the difficulty of hydrolysis at a carbonyl carbon of an α/β -unsaturated system is overcome by an enol-to-keto tautomerization of the dioate moiety, generating a 2,6-dioxo isomer that acts as the electron sink for a leaving carbanion^{15,16} (Scheme 1). Moreover, substrate destabilization

Scheme 1. Simplified Mechanisms Proposed for C–C Bond Hydrolysis by MCP hydrolases



preceding tautomerization has been observed during BphD-catalyzed hydrolysis of HOPDA.¹² Accordingly, the appearance of two distinct absorbing species (λ_{max} 473 and 492 nm) with 39 and 58 nm bathochromic-shifts were together named ES^{red}. The lifetime of this intermediate was extended by substitution of the catalytic serine in BphD (S112A)¹⁴ and HsAD from *Mycobacterium tuberculosis* (S114A).¹⁷ Crystallographic characterization of these ES complexes revealed that the presumably productive conformation of the MCP is nonplanar and includes a gauche+ torsion angle around the C4–C5 bond, represented in the two-dimensional Scheme 1 as a (3E)-2,6-dioxo isomer. In these complexes, the C2-oxo approaches the catalytic histidine, which may contribute to substrate destabilization. Nevertheless, the identity of ES^{red} is unknown, although double bond strain has most recently been proposed as the source of the spectral shift.^{12,17} In contrast, the S112A/H265A double variant did not trap the red-shifted intermediate, consistent with crystallographic characterization of a S112A/H265A:HOPDA complex, which revealed a planar binding mode with the C2-substituent orientated away from residue 265.¹⁴

Several experiments probing the mechanism of C–C bond hydrolysis in MCP hydrolases have led to the proposal that these enzymes are among the α/β -hydrolases that utilize a general base mechanism of catalysis (Scheme 1). Specifically, the catalytic triad has been proposed to activate H₂O, which attacks the substrate to form a *gem*-diolate intermediate. The strongest arguments for this intermediate have been based on two studies. First, studies of MhpC in H₂¹⁸O resulted in 3–6% incorporation of a second ¹⁸O equivalent into the succinic acid product during turnover of the enzyme's natural substrate, as well as an enzyme-dependent ¹⁸O exchange into a non-

hydrolyzable substrate analogue.¹⁸ Second, a broad ¹³C NMR signal at 128 ppm observed during the turnover of 6-¹³C-labeled HOPDA by each of three catalytically impaired MCP hydrolases (BphD H265A, BphD S112A, and MhpC H114A) was assigned to a *gem*-diolate.¹⁹ However, the report on the incorporation of 2 equivalents of ¹⁸O into the succinic acid product did not test for turnover-independent exchange into product. Moreover, the assignment of the putative *gem*-diol intermediate to the signal at 128 ppm is complicated by poor signal-to-noise as well as the presence of a signal with the same chemical shift in the substrate sample. The NMR studies are further complicated by the fact that the S112A and H265A variants accumulate spectroscopically distinct intermediates.¹⁴ Overall, the catalytic mechanism of the MCP hydrolases has not been definitively established.

Herein, the catalytic mechanism of MCP hydrolases has been investigated using BphD from *B. xenovorans* LB400 with a combination of rapid-scanning UV-visible absorption spectrophotometry, X-ray crystallography, positive ion electrospray tandem mass spectrometry (ESI/MS/MS) for peptide matching, and electron ionization gas chromatography–mass spectrometry (EI/GC/MS). An updated mechanism for the MCP hydrolases has been proposed. The mechanism is discussed within the context of C–C bond hydrolysis, and the chemical capabilities of the α/β -hydrolase triad are compared to those of the serine proteases. The versatility of the Ser-His-Asp triad is highlighted through discussion of its nucleophilic and general base-associated properties.

RESULTS

Identification of an Acyl-Enzyme Intermediate. To further investigate the role of the catalytic His in MCP hydrolases, His265 of BphD was substituted with glutamine, a relatively isosteric residue, as a single-point mutation or in tandem with an S112A mutation. The variants were purified and crystallized using microseeding, and X-ray diffraction data were obtained with and without exposing crystals to excess HOPDA. A 1.6 Å resolution crystal structure of H265Q incubated with HOPDA revealed clear electron density extending from the catalytic serine, which was unambiguously fit with a benzoyl moiety at full occupancy (Figure 1A). The benzoyl-oxo forms hydrogen (H-) bonds with the amides of each of the ‘oxyanion hole’ residues, Met113 and Gly42. The side chain of Gln265 is also oriented by polar contacts, including an H-bond between the Gln265 N^{e2} and O^{δ2} of Asp237 of the catalytic triad. Additional H-bonding linking Gln265 O^{e1} and Asn111 N^{δ2} is also possible. Gln-Asp effectively constitute a dyad, with no apparent interactions with the Ser-benzoyl moiety, which is located more than 4.5 Å from the N^{e2} of Gln265. Interestingly, a HOPDA molecule was bound at reduced occupancy in a secondary site, adjacent to the active site, and may represent an entry/exit pathway for the substrate and/or products (Figure S1A). This latter HOPDA was refined as a (3E,SZ)-2-oxo-6-oxido dianionic species (Table S2). The molecule is bound at the periphery of the P-subsite, and makes contacts with Gly41, Gly47, Ser50, Arg190, and a water molecule that is H-bonded to Gly43 (Figure S1B).

To investigate whether acylation also occurs in solution, chemical quench experiments were performed during turnover of a 5-fold excess of HOPDA by the wild-type (WT) and H265Q variant. LC ESI/MS analyses of the quenched reactions indicated that ~40% of the variant was benzoylated (M + 104) after 600 ms while ~45% of the WT was benzoylated after 200

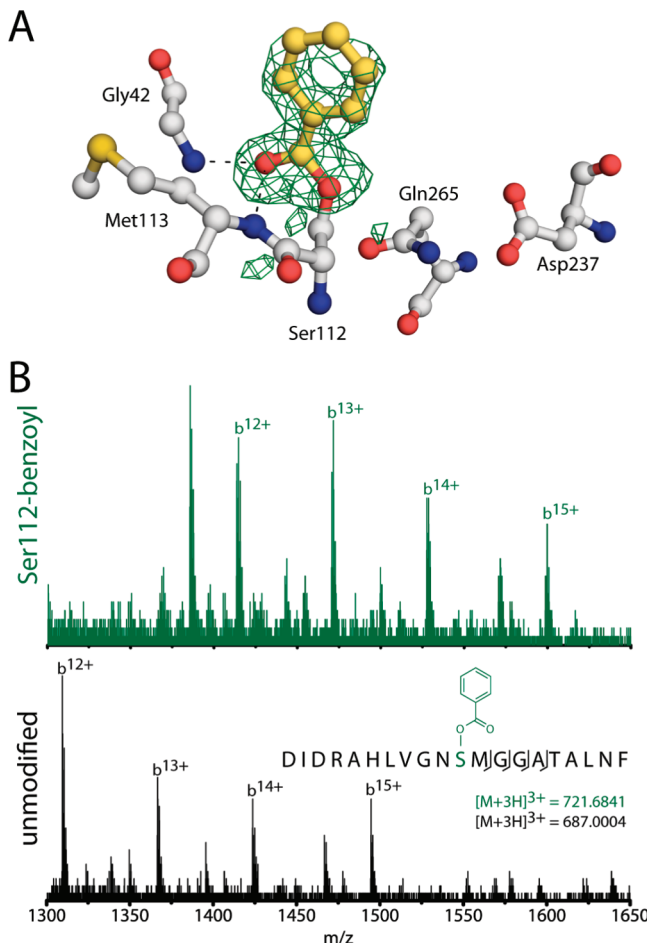


Figure 1. (A) Ball-and-stick representation of the H265Q:HOPDA complex active-site, including the unbiased $F_o - F_c$ density (green) at 3σ . Hydrogen bonding is indicated between the oxyanion hole residues and benzoyl moiety. (B) ESI/MS/MS of a modified and an unmodified peptide isolated from the wild-type sample. For simplicity, the high m/z range is shown, highlighting the differences in large *b*-series ions.

ms (Figure S2A,B). In WT-catalyzed reactions, ~30% of the enzyme was acylated after 1 s and no acylated enzyme was detected after 10 s (Figure S2C,D). The observed decay of the acylated species in WT BphD is consistent with the k_{obs} of 3.2

s^{-1} measured in kinetic burst experiments performed under similar conditions (*vide infra*).

Peptide matching from ESI/MS/MS of pepsin-digested reaction mixtures substantiated the acyl-enzyme intermediate identified in the H265Q crystal structure. The benzoylation of Ser112 was confirmed from a hydrophobic peptide spanning residues 102–120 (DIDRAHLVGNNSMGGATALNF), which contained several missed pepsin cleavage sites. Peptide fragment ions, matched in both the H265Q and WT samples, indicated modification of Ser112. In total, 6 ion fragments from the H265Q reaction mixture and 15 ion fragments from the WT sample were matched to *b*-series ions that could be explained only by benzoylation at Ser112 (Figure 1B, Table S3). The apparent stoichiometry of modified to unmodified peptide was consistent with the amount of benzoylation observed in the intact enzyme samples. Importantly, the X-ray diffraction and mass spectrometry data demonstrate that the Ser112-benzoyl intermediate forms under a variety of conditions. Together with the time-course data, this indicates that an acylated enzyme occurs on the reaction coordinate of BphD and perhaps other MCP hydrolases.

Stoichiometric ^{18}O Incorporation from H_2^{18}O Is Consistent with Nucleophilic Catalysis. Identification of an acyl-enzyme intermediate during the catalytic cycle of BphD conflicts with solvent ^{18}O exchange experiments performed using MhpC, which were used to infer a general base mechanism.¹⁸ To test whether BphD behaves similarly, 200 μM HOPDA was turned over using 20 μM BphD WT in potassium phosphate ($I = 0.1 \text{ M}$), pH 7.5 at 92% H_2^{18}O and the resulting benzoate was analyzed using EI/GC/MS. The observed distribution of ion fragments reflects both the extent of ^{18}O incorporation and the isotopic abundance of silicon in the derivatization agent. Therefore, the average distribution of ion fragments observed in control reactions performed using H_2O was used to calculate the extent of ^{18}O incorporation into benzoate observed in reactions performed in H_2^{18}O (Figure S3). In these calculations, two models were fit to the observed benzoate fragment ion distributions: a two-species model, representing a single ^{18}O incorporation event; and a three-species model, representing single and double incorporation events (Table S4). In turnover experiments performed using H_2^{18}O , the two-species model best fit the data. The result for the most abundant fragment, summarized in Table 1, indicates $85 \pm 1\%$ incorporation of a single ^{18}O equivalent. Similar results were observed in all other oxygen-containing fragments

Table 1. Enzymatic and Nonenzymatic Incorporation of ^{18}O from H_2^{18}O into Benzoate and HOPDA^a

sample and incubation time		relative abundance (%) of benzoate base peak ions (m/z)						^{18}O incorporation
		179 [M]	180 [M + 1]	181 [M + 2]	182 [M + 3]	183 [M + 4]	184 [M + 5]	
benzoate		H ₂ O	83.2	12.9	3.4	0.44		
WT + benzoate	300 min	H ₂ ¹⁸ O	83	12.3	4.3	0.4		ND ^b
WT + HOPDA	20 min	H ₂ ¹⁸ O	12	2.7	71	10.7	3.6	0.3
WT + HOPDA	20 min PI ^c	H ₂ ¹⁸ O	16.7	3.3	65	10	4	0.5
	20 min rxn							79 ± 2%
sample and incubation time		relative abundance (%) of HOPDA base peak ions (m/z)						^{18}O incorporation
		245 [M]	246 [M+1]	247 [M+2]	248 [M+3]	249 [M+4]	250 [M+5]	
HOPDA	20 min	H ₂ O	78	16	5	0.5		
		H ₂ ¹⁸ O	65	12.7	17.9	3.2	1.0	0.12
								18 ± 1%

^aA complete table of GC/MS results including additional fragments is available in the Supporting Information (Figure S3 and Table S5). Errors for ^{18}O incorporation represent the rms error from fitting the experimentally observed data to a single ^{18}O incorporation event. ^bND: not detected. ^cPI: HOPDA was preincubated in ^{18}O -buffer for the stated time prior to initiating the reaction (rxn).

Table 2. Kinetic Data for Wild-Type BphD and Its His265 Variants^a

enzyme	λ (nm)	k_1 (s^{-1}) [% Amp]	k_2 (s^{-1}) [% Amp]	k_3 (s^{-1}) [% Amp]	k_4 (s^{-1}) ^b [% Amp]
WT ^c	270		48 ± 12 [89]	8.3 ± 0.7 [11]	
	492	~500	54 ± 4 [64]	5.8 ± 0.7 [32]	
H265A ^d	434	78 [82]	1.3 [18]		0.0058
	270		10.8 ± 0.6 [28]	0.08 ± 0.02 [72] ^e	3×10^{-5}
H265Q	270		10.3 ± 0.1 [21]	0.022 ± 0.001 [64] ^f	
	434	130 ± 10 [16]			

^aEnzymes were reacted in 2:1 molar excess to HOPDA based on protomer concentration. ^b k_4 values were measured using a Cary5000 spectrophotometer. ^cFrom ref 12. ^dFrom ref 14. ^eThe error associated with the % Amp of k_3 is ~28% for H265Q at 270 nm, likely due to the competing process associated with enzymatic enolization, $k \sim 0.6 s^{-1}$, a faster process than HPD formation/release (k_3). ^fThe end point of the reaction was fixed at A434 nm = 0.006, consistent with the measured end point.

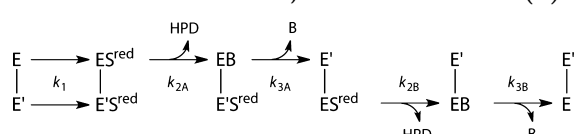
(Table S5), with approximately 85% of benzoate containing a single ¹⁸O equivalent. Importantly, this experiment provided no evidence for the enzymatic incorporation of a second ¹⁸O equivalent into the benzoic product: in no case were ions at M + 6 and M + 7 observed, and modeling incorporation of a second ¹⁸O equivalent into even a small percentage of the benzoate increased the error associated with the overall relative abundance of the singly exchanged species. For example, using the data presented in Table 1, modeling incorporation of a second ¹⁸O equivalent into 3% of the benzoate increased the error associated with the overall relative abundance of the single exchanged species by 5-fold (Table S4). Although BphD catalyzed the incorporation of a single equivalent of ¹⁸O into benzoate during hydrolysis of HOPDA, the enzyme did not catalyze any detectable solvent exchange into benzoate, even over 300 min (Table 1). However, nonenzymatic ¹⁸O exchange from solvent into HOPDA was observed at 18% over 20 min (Table 1). Interestingly, this exchange occurred exclusively at the C2-substituent (Figure S3E) suggesting that HOPDA exists predominantly as a 2-oxo-6-oxido-3,5-dienoate in solution. The preincubation of HOPDA in ¹⁸O-buffer for up to 20 min did not increase the stoichiometry of incorporation observed into the benzoic acid product, consistent with the finding that the nonenzymatic exchange into HOPDA was at the C2-oxo. Overall, the results are consistent with the occurrence of an acyl-enzyme intermediate.

The Role of the Catalytic His in Acylation and Deacylation. Identification of the acyl-enzyme substantiates the proposed assignment of rates observed during the turnover of HOPDA by WT BphD (Table 2).¹² Thus, the biphasic decay of ES^{red}, which initially forms at a rate of approximately 500 s^{-1} (k_1 , a measurement limited by the instrument dead time at 25 °C), could be unambiguously assigned to acylation (k_2 and k_3). The biphasic decay of ES^{red} is mirrored by an increase in absorbance at 270 nm due to the formation of HPD, which has been previously attributed to a two-conformation model of catalysis¹² (Scheme 2).

To evaluate the role of the catalytic His in these steps, we monitored turnover of HOPDA by a 2-fold excess of the

H265Q variant. As in the previously characterized H265A variant, H265Q did not accumulate ES^{red} (Figure S4A,B). Instead, the first observable phase during the turnover of HOPDA was a hyper- and small hypsochromic shift to 430 nm. The observed changes to the absorption spectrum are consistent with binding of a dianionic enolate substrate. Thereafter, the absorbance centered near 430 nm decayed in two phases as in the wild type, both of which were assigned to acylation. The first phase proceeded at a rate of 10.3 s^{-1} , approximately 5-fold slower than the first phase of ES^{red} decay for the wild type and 8-fold faster than enolate decay in the H265A variant (Figure S4C,E). The assignment of the first phase to acylation was corroborated by (a) monitoring HPD formation at 270 nm, which initially proceeded at a nearly equivalent rate of 10.6 s^{-1} (Figure S4F), and (b) chemical quenching, which established that close to half of the enzyme was acylated after this step. Inspection of the reaction for a longer time period suggested the conversion was complete but slowed by 2 orders of magnitude to a rate of 0.08 s^{-1} (Figure S4D). A corresponding k_3 was observed by monitoring the decay of the enolate. This rate, 0.022 s^{-1} , is approximately 4-fold faster than that reported for the H265A variant, and is 2 orders of magnitude slower than wild-type catalysis. This slower phase presumably corresponds to acylation at active sites that require deacylation or product release dependent on a change in conformation. H265Q (2–4 μ M) catalyzed the turnover of saturating amounts of HOPDA (50 μ M) at a rate corresponding to a k_{cat} of ~3 × 10⁻⁵ s^{-1} . This slow rate was not detected under single turnover conditions. Overall, these data indicate that the catalytic histidine plays a more important role in deacylation than in acylation. Moreover, this interpretation corroborates the assignment of the two phases of ES^{red} decay during WT turnover to acylation events.

The Role of the Catalytic His in Forming ES^{red}. As noted above, the H265Q variant did not accumulate ES^{red} during the turnover of HOPDA. The effect of glutamine substitution on HOPDA binding was further probed using the catalytically inactive S112A/H265Q variant. Upon mixing HOPDA with a 2-fold excess of enzyme in potassium phosphate ($I = 0.1$ M), pH 7.5, a hyper- and slight hypochromatic shift to 432 nm was observed (Table S6). The resulting ES complex accumulated over approximately 20 min until reaching 125.0 ± 0.9% of the initial absorptivity, $\epsilon_{434\text{ nm}} = 32.1 \pm 0.2 \text{ mM}^{-1} \text{ cm}^{-1}$ (Figure S5B,C). These changes to the absorption spectra suggest preferential binding of a dianion, which was initially present as only 63% of the sample (pK_{a2} HOPDA = 7.3). Curiously, the hyperchromic shift accounted for only half of that expected for a complete conversion to an all enolate sample, $\epsilon_{434\text{ nm}} = 40.1 \text{ mM}^{-1} \text{ cm}^{-1}$ at pH 9.5 (>99% HOPDA²⁻). Incubation of HOPDA with a 2-fold excess of S112A/H265Q in Na-CHEs (I



^aThe rate constants denoted by alphabetical subscripts distinguish equivalent sites within an MCP hydrolase tetramer.

= 0.1 M), pH 9.5, shifted the enolate band to 432 nm with no significant change in the intensity. At pH 7.5 a lower bound for the half-life of the S112A/H265Q-bound HOPDA was estimated at 31 ± 2 h.

An X-ray structure of an S112A/H265Q:HOPDA complex was obtained and refined to 1.9 Å resolution with the HOPDA modeled at 60% occupancy. Refinements in the absence of planarity restraints affecting the C2–C3, C3–C4, C4–C5, or C5–C6 bonds indicated a (3E,5Z)-2-oxo-6-oxido-dienoate was compatible with the X-ray data (Table S2), although refinements in the presence of planarity restraints and analysis of electron density maps could not eliminate the binding of a (2E,4E)-2-hydroxy-6-oxo- or a (3E)-2,6-dioxo isomer. The latter isomers were disfavored in light of visible absorption spectra observed in solution and the results of refinements without planarity restraints. This conclusion was validated by observations of solvent ^{18}O exchange into the substrate.

The observed binding mode, in which the dienoate carbons, C1 to C6, are coplanar, is stabilized in part by a number of polar contacts (Figure S5A). In particular, the 6-oxido group is H-bonded to both the ‘oxyanion hole’ amides. At the P-subsite, the HOPDA carboxylate hydrogen bonds with Gly43, Arg190, Trp266 and a water molecule that can also H-bond with Gly41, Asn51, and Asn111. In the absence of HOPDA, a second water molecule (not shown) replaces the interactions of a carboxylate oxo-group in the P-subsite. The orientation of the planar (3E,5Z)-2-oxo-6-oxido isomer and its interaction with the active site differ significantly from the observed binding mode in the S112A:HOPDA complex, which has been fit to a nonplanar (3E)-2,6-dioxo isomer. The most significant differences are at the P-subsite, wherein the double variant features an H-bond between the C2-oxo and Arg190 and an additional water molecule anchoring the carboxylate, as described above (Figure 2). Two ($F_o - F_c$) difference electron density features approximately the size and shape of a phenylalanine side chain are also observed in a nonpolar surface pocket bounded largely by the side chains of Ile153, Phe157, Phe204, and Leu205 near the periphery of the NP subsite. These features approach within 5 and 7 Å of the active site HOPDA’s phenyl group and may represent the phenyl groups of additional HOPDA molecules with disordered dienoate groups, although this interpretation is not incorporated into the refined atomic model. Coupled with the additional HOPDA density observed at the opposite side of the active site in the H265Q:HOPDA structure, it appears that BphD may have two routes for substrate/product entry/egress.

The Pre-Steady-State Kinetic Burst Suggests BphD Is Half-Site Reactive. The observation of an acyl-enzyme prompted us to investigate the occurrence of burst kinetics using stopped flow spectrophotometry. Multiple turnover reactions, monitored at 270 nm, were performed using 1, 2, or 4 μM WT BphD and a saturating amount of HOPDA (40 μM). The resulting pre-steady-state kinetic burst was ascribed to HPD formation, and quantified ($\epsilon_{270\text{ nm}}^{\text{HPD}} = 19.2\text{ mM}^{-1}\text{ cm}^{-1}$) as previously reported.²⁰ Values derived from fitting the measurements to a burst equation are summarized in Table 3 (Figure S6). The presence of a burst phase is consistent with a covalent mechanism in which acylation is not rate-limiting. The pre-steady burst rate, $k_{\text{burst}} \sim 55\text{ s}^{-1}$, is in agreement with the faster phase of ES^{red} decay, assigned to acylation, $k_2 \sim 50\text{ s}^{-1}$. Interestingly, the magnitude of the burst accounted for only half the enzyme used in each assay, suggesting that BphD may be a half-site reactive enzyme.

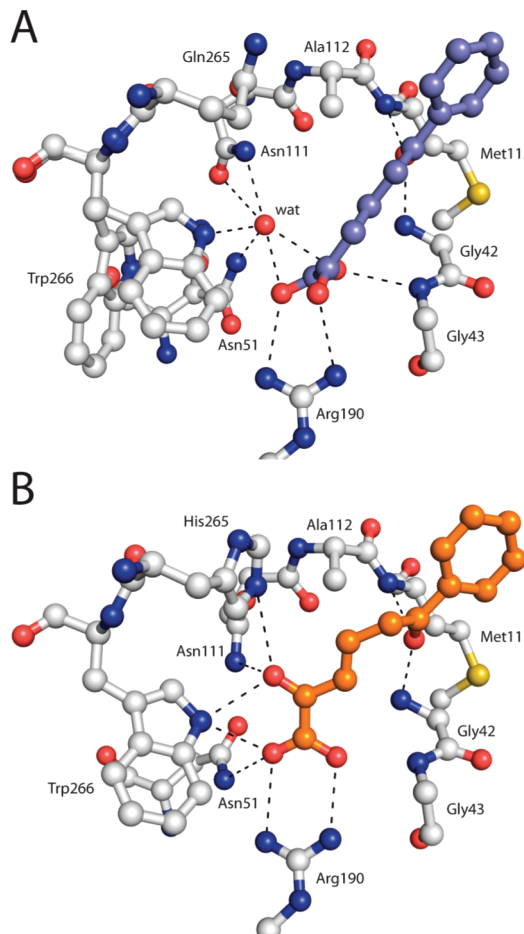


Figure 2. Ball-and-stick representations of the stable HOPDA binding modes observed in crystalline ES complexes. Polar contacts equal to or less than 3.4 Å are drawn as dashed lines. (A) The planar dienoate, ES_{planar}, bound to BphD S112A/H265Q showing an additional water molecule in the P-subsite, below the dienoate plane. (B) The nonplanar, electronically excited species, ES^{red}, bound by BphD S112A (PDB ID: 2PUH).¹⁴

DISCUSSION

The presented chemical quench data provide direct evidence for the occurrence of a covalent catalytic intermediate in a wild-type MCP hydrolase: not only was the Ser112-benzoyl species observed by mass spectrometry, but it formed and decayed on a time scale consistent with turnover. A weak NMR signal has been attributed to a *gem*-diol intermediate, but has only been reported in catalytically impaired variant enzymes.¹⁹ The direct observation of a covalent intermediate reported herein is substantiated by three independent lines of evidence: (i) the observation of an acyl-enzyme *in crystallo* using the H265Q variant, (ii) the existence of a pre-steady-state kinetic burst, and (iii) incorporation of a single equivalent of ^{18}O into benzoate when HOPDA was hydrolyzed by BphD WT in H_2^{18}O .

The stoichiometric incorporation of ^{18}O from solvent into benzoate by BphD contrasts to a study of MhpC, in which 3–6% of its MCP acid product, succinate, contained two ^{18}O equivalents.¹⁸ The MhpC study did not report on the possibility that MhpC catalyzes ^{18}O incorporation into succinate. Significantly, aspartyl and serine proteases both exchange ^{18}O into their acid products despite using different catalytic mechanisms for hydrolysis.^{23–25} While BphD did not catalyze solvent exchange into benzoate, differences between

Table 3. Pre-Steady-State Kinetic Parameters Derived from Monitoring HPD Formation at 270 nm

[E] (μM)	$k_{\text{burst}} (\text{s}^{-1})$	$\Delta A_{270 \text{ nm}}$	[P] _{burst} (μM)	$k_{\text{ss}} (\Delta A_{270 \text{ nm}}, \text{s}^{-1})$	$k_{\text{ss}} (\text{s}^{-1})$
1	52 ± 5	0.0098 ± 0.0007	0.51 ± 0.04	0.081 ± 0.007	4.2 ± 0.4
2	55 ± 5	0.0199 ± 0.0008	1.04 ± 0.04	0.150 ± 0.003	3.91 ± 0.08
4	62 ± 1	0.0376 ± 0.0007	1.96 ± 0.04	0.243 ± 0.004	3.16 ± 0.05

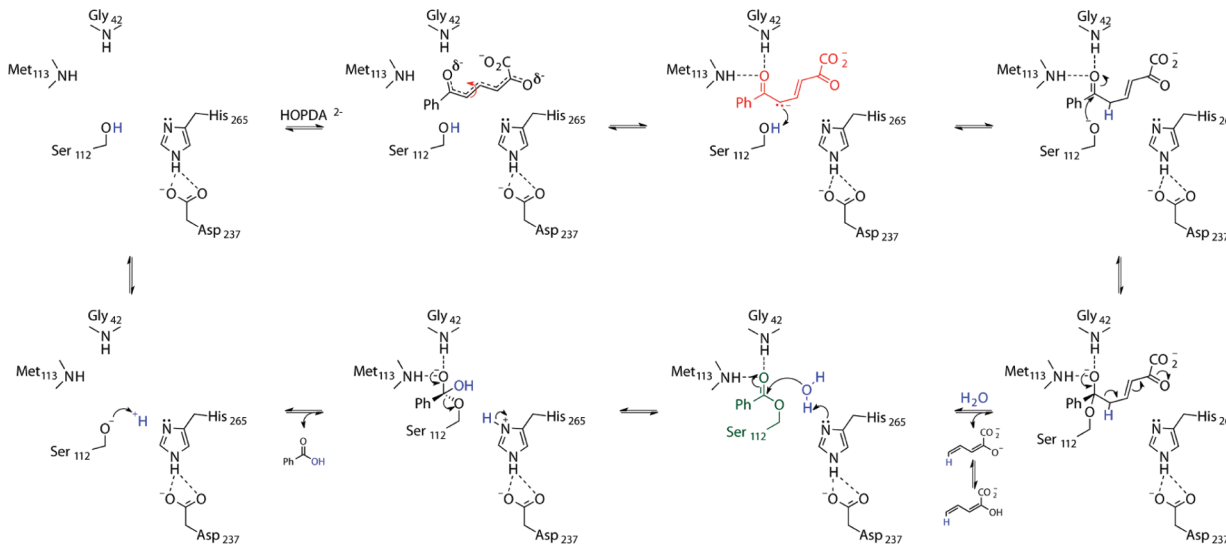


Figure 3. An updated mechanism for the MCP hydrolases. A complete catalytic cycle is shown, beginning with binding of a HOPDA dianion of undefined electronic and geometric structure. Rotation about C4–C5 is indicated using a red arrow. The intermediate ES^{red} , shown in red, is hypothesized as a carbanion. The proposed fate of H_2O is shown in blue, and the observed acyl-enzyme intermediate is colored green.

the systems may account for the differential incorporation of ^{18}O into the carboxylates. First, several distinct binding modes have been observed for succinate and malonate in complex with MhpC H263A¹³ and BphD,²¹ respectively, indicating that small diacids interact with the hydrolase active site differently than monoacids such as benzoate. Furthermore, MhpC contains an additional active site histidine, His114, which contributes²² to catalysis and coordinates succinate *in crystallo*.¹³ This residue, which corresponds to Ala116 in BphD, may influence the reactivity of small diacids with MhpC.

On the basis of the evidence presented herein, an updated mechanism of catalysis, illustrated using BphD as the reference MCP hydrolase, is proposed in Figure 3. The active site architecture and observed binding phenomena suggest preferential binding of a dianionic HOPDA isomer. Proximity of the lone pair of electrons on the His265 N^{e2} to the substrate's C2-carbonyl is likely to favor localization of negative charge away from the C2-carbonyl group. Importantly, a gauche conformation around the C4–C5 bond is required to maintain all interactions with the NP- and P-subsites, implying generation of an sp³-hybridized carbon at C5, consistent with an enol-to-keto tautomerization. As presented below, we propose that ES^{red} is an sp³-hybridized C5 carbanion and that tautomerization is completed via protonation at C5 by the nearby Ser112. This tautomerization generates the requisite electron sink for C–C bond cleavage. The resulting serinate then attacks the C6-carbonyl, generating the first tetrahedral oxyanion intermediate that collapses to a Ser112 benzoyl-ester and HPD. Presumably, the His265 N^{e2} lone pair also serves a role in destabilizing binding of the resulting HPD to accelerate its release. Upon binding of H_2O to the acyl-enzyme, the His-Asp dyad acts as a general base to activate water. Attack on the acyl-enzyme then generates the second tetrahedral oxyanion

intermediate, which ultimately leads to benzoate production. At the end of the catalytic cycle, protonation of Ser112 regenerates the resting state enzyme. For the MCP hydrolases, it is unclear whether the rate-limiting step, k_{cat} or k_3 , represents deacylation or a conformational change preceding final product release.

Despite sharing catalytic machinery and an acyl-enzyme intermediate, the MCP hydrolases and serine proteases are strikingly different with respect to the mechanism of nucleophile activation. Kinetic characterization of the H265Q and H265A¹⁴ BphD variants suggests that the rate of acylation is only affected 5- to 40-fold by substitution of the catalytic histidine. In the case of H265Q, this was confirmed by mass spectrometry of a chemically quenched reaction mixture. Moreover, a BphD D237N variant behaved similarly to His265 variants during single turnover experiments, exhibiting a hyperchromic-shifted enolate spectrum and a slower rate of acylation.¹⁹ This indicates that the catalytic histidine contributes little to serine activation in MCP hydrolases, in contrast to what has been proposed for serine proteases.^{26,27} In the MCP hydrolases, activation of the serine appears to be substrate-assisted. Thus, an accumulation of negative charge on C5 facilitates the rotation about the C4–C5 bond in order to satisfy the full suite of enzyme–substrate interactions, and in turn activates Ser112 by a proton transfer that completes substrate tautomerization. Overall, the results suggest that the acylation reaction in the MCP hydrolases does not depend on the ‘charge relay system,’ originally described in the context of the serine protease, and instead depends on exploiting the ability of the substrate’s conjugated system to reposition charge throughout the course of the reaction.

The tautomerization catalyzed by the MCP hydrolases is a two-step process in which the substrate is destabilized to form ES^{red} prior to protonation by the serine. Disruption of the His-

Asp dyad dramatically affects the substrate destabilization that leads to production of ES^{red} , although the histidine is not absolutely required for tautomerization. If we consider the S112A variant as a good model of the wild-type enzyme due to its ability to stabilize the activated substrate, then the binding mode of HOPDA in S112A is expected to mimic that of the wild type. Binding of the HOPDA as a (3*E*)-2,6-dioxo- isomer positions the C2-carbonyl \sim 3 Å from the His265 N^{e2} lone pair, which likely contributes to electronic destabilization. In the ES complexes of H265X/S112A variants, the HOPDA binding mode differs remarkably in that it is probably a fully planar, (3*E*,5*Z*)-2-oxo-6-oxido isomer, in which the C6-oxido is positioned directly between the ‘oxyanion hole’ amides. The HOPDA is also accompanied by an additional water molecule that facilitates different contacts with P-site residues. Disruption of the binding mode is reflected in the spectrophotometric experiments by the absence of ES^{red} . It is therefore conceivable that ES^{red} is formed at a much slower rate in the His-Asp dyad variants. Reduction of the rate constant by at least 2 orders of magnitude relative to wild-type turnover (where $k_1 \sim 500 \text{ s}^{-1}$) would be consistent with the inability to detect the intermediate spectrophotometrically, and suggests that ES^{red} formation may limit the rate of acylation in these variants. Thus, the rate constant denoted as k_2 for the His variants may represent generation of ES^{red} . Accordingly, any signal from ES^{red} would be quenched through rapid protonation by Ser112.

The proposal that ES^{red} represents an enzyme-stabilized C5 carbanion is more consistent with the available experimental data than either of two previous proposals. In one of these, ES^{red} was assigned as a strained (2*E*,4*E*)-2-oxido-6-oxido-dienoate.¹⁷ Nevertheless, crystallographic analyses of ES complexes suggest that the intermediate is more consistent with the (3*E*)-2,6-dioxo isomer. A second hypothesis acknowledging the results of restrained refinements of the dienoate is polarization of the π electrons of an α,β -unsaturated ketone. In fact, binding of an inhibitor to crotonase resulted in a 90 nm bathochromic shift.²⁸ Nevertheless, such a polarization in MCP hydrolases would represent a red-shift greater than 220 nm from the expected λ_{max} of HPD, raising the energy of the system by \sim 48 kcal/mol. An enzyme-stabilized C5 carbanion is compatible with the results of the restrained refinements of MCPs to (3*E*)-2,6-dioxo isomers. Mechanistically, such a carbanion is consistent with the negative charge that must accumulate on C5 for substrate tautomerization. While enzymatic carbanion formation is typically energetically unfavorable, it is only \sim 9 kcal/mol for an enolate,²⁹ and delocalization into a carbonyl stabilized by coordination to a Lewis acid, such as an ‘oxyanion hole’, is a common catalytic motif.³⁰ Additionally, the requisite energy could be easily supported by the large number of polar and nonpolar contacts in the active site (Table S7). The theoretical change in energy associated with a 58 nm transition is \sim 7.8 kcal/mol, comparable to the energy required to stabilize an enolate carbanion. Finally, the spectrophotometric contribution of a carbanion is also consistent with a red-shifted intermediate, explained by an n to π^* transition. A similar, 50 nm bathochromic shift was observed between different species of triphenylmethyl lithium: the contact ion pair exhibited a λ_{max} at 446 nm, whereas the absorption spectra of the solvent separated ion pair was centered around 496 nm.³¹ Despite consistency with the observed data, the absence of any direct evidence makes any assignment of ES^{red} provisional.

Assignment of the observable catalytic steps implicates His265 as a general base required for efficient breakdown of the acyl-enzyme intermediate. The role of the catalytic histidine in activating water for hydrolysis of the ester bond further establishes the versatility of the α/β -hydrolase superfamily’s catalytic triad to activate small molecules. Similarly, an alcohol is activated during the reaction catalyzed by DAC-AT. Indeed, a structure of the acetylated DAC-AT:deacetyl-cephalosporin complex provides significant insight into the mechanism of deacylation of MCPs (Figure S7). Superposition of a wild-type structure of BphD (PDB ID: 2OG1, chain B¹²) and the H265Q acyl-enzyme revealed that the His is positioned \sim 3.3 Å from the ester, comparable to the distance in the DAC-AT structure. In both structures, the ‘oxyanion hole’ residues are well-positioned for stabilization of a tetrahedral oxyanion intermediate during breakdown of the acyl-enzyme. An apparently short hydrogen bond between His265 and Asp237 (\sim 2.5 Å) in this structure of wild-type BphD is analogous to structures observed in the serine proteases. Interestingly, the His-Asp pair is required for deprotonation of the nucleophilic serine in the serine proteases, which proceeds in the MCP hydrolases even upon disruption of the dyad chemistry.

The magnitude of the pre-steady-state burst in BphD is consistent with a mechanism of covalent catalysis in which a process subsequent to acylation is rate-limiting. Thus, quantification of HPD produced during the burst corresponded to only half of the available hydrolase active sites. Moreover, the relative ratio of modified to unmodified enzyme and peptides was also more consistent with half-site reactivity, a feature of MCP hydrolases first proposed by Bugg and his co-workers based on the half-site occupancy of an MhpC tetramer complexed with an inhibitor.¹¹ This phenomena has since been observed in two HsaD:MCP complexes.¹⁷ Unfortunately, crystallographic symmetry of all BphD–substrate complexes requires equivalence across all active sites, which limits information regarding differential active site binding affinities.^{12,14,21} Nevertheless, even in cases where substrate binding is stoichiometric, reactivity may not be concomitant. Most recently, this has been demonstrated in LuxG, a full-site binding, half-site reactive flavin reductases.³² For BphD, the two-conformation model provides a more satisfactory explanation for the biphasic formation of HPD, in which benzoate release coupled with subunit communication is described as the rate determinant during hydrolysis.¹²

■ CONCLUSION

The current study establishes that the MCP hydrolases utilize a covalent mechanism of catalysis to hydrolyze a C–C bond at a carbonyl carbon of an α/β -unsaturated system. Furthermore, the quantification of the kinetic burst associated with acylation indicates that BphD is half-site reactive, a rarely observed phenomenon. While MCP hydrolases represent another example of the convergent evolution of the catalytic Ser-His-Asp triad in nature, their chemistry deviates from the classical serine protease mechanism. Indeed, family specific enzyme–substrate interactions dictate the family specific mechanism. In the case of MCP hydrolases, tautomerization of the dienoate substrate serves dual functions: generating an electron sink for hydrolysis and activating the nucleophile, replacing the catalytic triad’s ‘charge-relay system’ in this role. More specifically, the His-Asp dyad catalyzes this first half-reaction to generate an intermediate with a bathochromically shifted spectrum, which in turn activates the serine for nucleophilic attack on the

substrate's carbonyl. To the best of our knowledge, the proposal of this carbanion as the source of the spectral shift in the intermediate is biologically unprecedented. Current studies are aimed at substantiating the nature of this intermediate.

EXPERIMENTAL SECTION

Preparation of Enzymes and Substrate. BphD variants were generated using a broad host range plasmid carrying *bphD* (pSS184) or *bphD* S112A (pSS184).¹⁴ Substitution of His265 to glutamine (H265Q) was performed using a 5'-phosphorylated primer (H265Q: PO₄-CTCCAAGTGC~~G~~GGCCAGTGGCGCAATGG) and the QuikChange Multi Site-Directed Mutagenesis Kit (Stratgene, La Jolla, CA). All enzyme concentrations reported refer to the monomer concentration, which was calculated using an extinction coefficient determined by amino acid analysis, $\epsilon_{280\text{ nm}} = 55.4 \text{ mM}^{-1} \text{ cm}^{-1}$. HOPDA was enzymatically generated from 2,3-dihydroxybiphenyl (DHB) using dihydroxybiphenyl dioxygenase as previously described.³³ All other chemical were of reagent grade.

Crystallization and Manipulation of Crystals. Crystals of BphD S112A/H265Q and H265Q were obtained at 20 °C via the vapor diffusion method using 24-well Cryschem sitting drop plates (Hampton Research, Aliso Viejo, CA). Initial crystallization experiments explored a grid of sodium malonate (2.4–3.3 M) against pH (6.0–7.0). Diffraction quality crystals of S112A/H265Q were first obtained at 2.4 M malonate after microseeding. Droplets containing protein (~4 mg/mL in 20 mM HEPES, pH 7.5) and reservoir solutions, 1 μL each, were equilibrated against reservoirs for 9 days prior to the addition of 1 μL of a seeding solution. A crystal of BphD S112A/H265A, grown as previously described,¹⁴ was crushed in 200 μL of its reservoir solution to prepare the seeding stock, which was serially diluted with reservoir solution by 10, 10², 10³, and 10⁴ to prepare seeding solutions. Needle-like crystals of H265Q were obtained in a parallel experiment using 1.4 mg/mL protein in 20 mM HEPES, pH 7.5. Reagents from the Hampton Research Additive Screen (HR2-428) were tested with both mutants. Addition of either ethylene glycol, 3% (v/v) in the crystallization droplet, or calcium chloride, 10 mM in the droplet, proved beneficial. Diffraction quality crystals of H265Q were obtained with either additive using 2.4 mg/mL protein without seeding. Table S1 characterizes the crystallization conditions for crystals used in the structure determinations reported below. Crystals were exposed to HOPDA in their original droplet of mother liquor by addition of 30 μL of 10–15 mM HOPDA dissolved in the crystal's reservoir solution and incubating for 60–150 min. Prior to flash-freezing by immersion in liquid nitrogen, substrate free crystals were passed rapidly through a reservoir wash, a 1:1 reservoir/cryoprotectant wash, and finally into the cryoprotectant (3.5 M sodium malonate, pH 6.3). Crystals exposed to HOPDA were harvested into a drop containing equal volumes of the HOPDA stock solution and the cryoprotectant and transferred into the cryoprotectant.

Structure Determination and Analysis. All diffraction experiments were performed under cryogenic conditions (100 K). The resolution and other qualities of the diffraction patterns were first assessed using an R-axis IV++ diffractometer (Rigaku) and Cu-Kα radiation prior to acquisition of complete patterns using synchrotron radiation at the Advanced Photon Source (APS) of Argonne National Laboratory. The diffraction images were processed using HKL2000: indexing and integration by XDisplayF and DENZO, scaling and averaging by SCALEPACK.³⁴ Programs from the CCP4 suite were used for most crystallographic calculations.³⁵ Initial atomic models were obtained by molecular replacement using modified versions of previously determined structures of BphD (e.g., PDB entry 2PUS, chain A). To prepare search models, COOT³⁶ was used to: remove all nonprotein atoms, adjust the occupancies of side chain atoms in residues with alternative conformations to 0.02 beyond Cβ, and set all B-factors to 20.0 Å². Iterative cycles of model building and refinement utilized COOT and REFMAC.³⁶

All other PDB files were downloaded from the RCSB Protein Data Bank, and pairwise superposition of structures was performed using the SSM Superposition tool³⁷ in COOT.³⁶

Restrained Refinement of HOPDA Isomers. HOPDA may be bound in several forms, including the keto and enol tautomers of the monoanion and the resonance structures of the enolate dianion. At this resolution, distinction between the possible structures relies on identification of C–C bonds that must be single bonds with torsion angles significantly different from 0/180°, and assessment of which multiatom groups can be planar and thus might be coupled by double bonds. To limit initial model bias, HOPDA was fit into the density and initially refined without enforcing strict double bond character at any bond: in the initial fitting, no bonds were forced to torsion angles of 0/180°, and in early refinement cycles, all torsion angles were treated as variable angles with high uncertainty and planarity was enforced only for the carboxylate and phenyl planes. In a second stage of refinement, the application of reduced levels of uncertainty in the torsion angles proved ineffective for distinguishing among possible structures. The final stage involved parallel refinements with planarity enforced about different bonds as appropriate for the keto tautomer, the enol tautomer, and its conjugate base (the 2-oxido-6-oxo isomer), and the 2-oxo-6-oxido form of the enolate (named HKE). The fit to the electron density and features of the (F_o – F_c), α_c difference electron density maps were assessed during each stage.

Rapid-Quench Methods. Acyl-enzymes were prepared using the sequential mixing option of an SX.18MV stopped-flow reaction analyzer (Applied Photophysics, Ltd., Leatherhead, U.K.). The temperature of the drive syringe chamber and optical cell were held at 25 °C by a circulating water bath. Samples analyzed by ESI/MS/MS originated from reactions of 4 μM enzyme and 20 μM HOPDA in potassium phosphate ($I = 0.1 \text{ M}$, pH 7.5) that were allowed to age for 200 or 600 ms for the wild type or H265Q variant, respectively, before quenching 1:1 with 10% acetic acid (v/v). Quenched samples were collected on ice, measured to be at pH 2.3, then concentrated at 4 °C. The concentrated samples were incubated with 1:50 pepsin (w/w) for 1 h at 37 °C. Digests were halted by flash freezing with liquid N₂, and the resulting peptide mixtures were stored at –20 °C until further analysis. Additional wild-type enzyme samples were prepared under identical reaction conditions with aging times of 0.2, 1, or 10 s. These samples, along with a 600 ms quench of the H265Q variant-catalyzed reaction, were kept intact, and analyzed by LC ESI/MS.

Mass Spectrometry of Enzyme Samples. Pepsin-digested peptides were analyzed by liquid chromatography–tandem mass spectrometry and identified exactly as previously described³⁸ except that pepsin specificity was used to limit the database search, benzoylated Ser was allowed as a variable modification, and the fragment spectra were searched against a library containing the BphD sequence. Whole protein samples were analyzed by HPLC-MS. The HPLC was equipped with a C₁₈ precolumn (Dionex) and the MS was a Q-TOF hybrid instrument (QSTAR, Pulsar i, Applied Biosystems, Foster City, CA). Briefly, reaction mixtures were loaded onto the precolumn, and the buffer salts were washed from the samples before elution in 80% acetonitrile, 0.1% formic acid. The modification observed in the resulting mass spectra was estimated by comparing peak areas calculated from a Gaussian peak fitting function in Origin 8.0 (OriginLab Corporation, Northampton, MA).

Solvent ¹⁸O Exchange and EI/GC Mass Spectrometry. For solvent exchange experiments, 20 μM BphD WT was incubated with 200 μM benzoate for 300 min or used to cleave 200 μM HOPDA over 20 min in 50 μL of potassium phosphate ($I = 0.1 \text{ M}$), pH 7.5, in 92% H₂¹⁸O. Benzoate samples were prepared in acetone, applied to microfuge tubes, and allowed to evaporate to dryness before incubation in ¹⁸O-buffer with or without enzyme. Quantified samples of HOPDA in potassium phosphate ($I = 0.1 \text{ M}$), pH 7.5, were lyophilized before resuspension in H₂¹⁸O with or without enzyme. In some instances, HOPDA was preincubated with the ¹⁸O-buffer for either 5 or 20 min prior to the addition of enzyme. The enzyme was prepared in natural abundance buffer. This buffer was also added to samples that did not contain any enzyme in order to account for the dilution of H₂¹⁸O to 92%. After incubation (20 or 300 min), samples

were simultaneously acidified to pH 2.3 with acetic acid (5% final v/v) and extracted with 2 vol (100 μ L) of ethyl acetate. The organic fraction was dried under vacuum and resuspended in 25 μ L of pyridine. The products were derivatized using an equal volume of BSTFA + TMCS (99:1) for at least 10 min. EI/GC/MS was carried out using an HP 6890 series GC system fitted with an HP 5973 mass selective detector and an HP 5 ms (30 m \times 250 μ M) column. The operating conditions were: T_{GC} (injector) 280 °C; T_{MS} (ion source) 230 °C; oven program time $T_{0\text{ min}}$ 80 °C, $T_{60\text{ min}}$ 290 °C, $T_{0\text{ min}}$ 80 °C (heating rate 5 °C min⁻¹). The retention time of TMS-derivatized benzoate and HOPDA were 13.2 and 35.4 min, respectively. The relative abundance of fragment ions is reported as the percentage of a single species and the error between two replicated is reported as a standard deviation. The average distribution of fragment ions observed in H₂O was used to estimate the amount of ¹⁸O incorporation by fitting the data in H₂¹⁸O to two distinct models accounting for (i) a single ¹⁸O incorporation event, and (ii) low level of incorporation of a second ¹⁸O equivalent into benzoate. The root-mean-square error is reported for each fit.

Rapid-Scanning Kinetics. The SX.18MV stopped-flow reaction analyzer equipped with a photodiode array was utilized to generate full spectrum scanning kinetic traces for the purpose of generating representative figures. All kinetic measurements were performed in potassium phosphate ($I = 0.1$ M, pH 7.5) at 25 °C. Experiments performed for more accurate determination of rates were performed using the monochromatic wavelengths stated (0.5 mm slit width). Single turnover experiments were performed at approximately 2:1 enzyme to HOPDA ratio; 8.1 μ M enzyme was reacted with 4 μ M HOPDA. Multiple turnovers were observed using the same instrumental setup. A pre-steady-state burst was monitored at 20 μ M HOPDA while varying the concentration of enzyme. All reported biological replicates refer to an average of at least 5 shots from the stopped flow, where each individual syringe, both enzyme and substrate, was prepared fresh before each replicate. At least three technical replicates were performed for each experiment, and errors are reported as standard deviation between replicates.

ASSOCIATED CONTENT

Supporting Information

Properties of crystals, diffraction data, and refinement statistics, results of restrained substrate refinement, MS results, ribbon and ball-and-stick drawings of ES complexes, representative stopped-flow kinetic traces and spectra, analysis of steady-state data, analysis of structural data. This material is available free of charge via the Internet at <http://pubs.acs.org>.

AUTHOR INFORMATION

Corresponding Author

jtb@purdue.edu; leltis@mail.ubc.ca

Present Address

¹Department of Chemistry, Wilfrid Laurier University, Waterloo, Ontario, Canada

Author Contributions

[‡]These authors contributed equally.

Notes

The authors declare no competing financial interest.

ACKNOWLEDGMENTS

We thank Drs. Martin Tanner and Shiva Bhowmik for helpful discussions as well as Dr. William Mohn for use of the GC/MS. The research was supported by a Discovery grant from the Natural Sciences and Engineering Research Council of Canada to L.D.E. Protein and peptide MS data were collected at UBC's Proteomics Core Facility by Jason Rogalski. X-ray diffraction data were obtained at the Southeast Regional Collaborative

Access Team (SER-CAT) 22-ID beamline at the Advanced Photon Source, Argonne National Laboratory. Supporting institutions may be found at www.ser-cat.org/members.html. Use of the Advanced Photon Source was supported by the U.S. Department of Energy, Office of Science, Office of Basic Energy Sciences, under Contract No. W-31-109-Eng-38.

REFERENCES

- (1) Holmquist, M. *Curr. Protein Pept. Sci.* **2000**, *1* (2), 209–35.
- (2) Ollis, D. L.; Cheah, E.; Cygler, M.; Dijkstra, B.; Frolov, F.; Franken, S. M.; Harel, M.; Remington, S. J.; Silman, I.; Schrag, J.; et al. *Protein Eng.* **1992**, *5* (3), 197–211.
- (3) Froede, H. C.; Wilson, I. B. *J. Biol. Chem.* **1984**, *259* (17), 11010–3.
- (4) Li, J.; Szittner, R.; Derewenda, Z. S.; Meighen, E. A. *Biochemistry* **1996**, *35* (31), 9967–73.
- (5) Nazi, I.; Wright, G. D. *Biochemistry* **2005**, *44* (41), 13560–6.
- (6) Rink, R.; Fennema, M.; Smids, M.; Dehmel, U.; Janssen, D. B. *J. Biol. Chem.* **1997**, *272* (23), 14650–7.
- (7) Lejon, S.; Ellis, J.; Valegard, K. *J. Mol. Biol.* **2008**, *377* (3), 935–44.
- (8) Bugg, T. D. *Bioorg. Chem.* **2004**, *32* (5), 367–75.
- (9) Nardini, M.; Dijkstra, B. W. *Curr. Opin. Struct. Biol.* **1999**, *9* (6), 732–7.
- (10) Jiang, Y.; Morley, K. L.; Schrag, J. D.; Kazlauskas, R. J. *ChemBioChem* **2011**, *12*, 768–76.
- (11) Dunn, G.; Montgomery, M. G.; Mohammed, F.; Coker, A.; Cooper, J. B.; Robertson, T.; Garcia, J. L.; Bugg, T. D.; Wood, S. P. *J. Mol. Biol.* **2005**, *346* (1), 253–65.
- (12) Horsman, G. P.; Ke, J.; Dai, S.; Seah, S. Y.; Bolin, J. T.; Eltis, L. D. *Biochemistry* **2006**, *45* (37), 11071–86.
- (13) Li, C.; Li, J. J.; Montgomery, M. G.; Wood, S. P.; Bugg, T. D. *Biochemistry* **2006**, *45* (41), 12470–9.
- (14) Horsman, G. P.; Bhowmik, S.; Seah, S. Y.; Kumar, P.; Bolin, J. T.; Eltis, L. D. *J. Biol. Chem.* **2007**, *282* (27), 19894–904.
- (15) Lam, W. W.; Bugg, T. D. *Biochemistry* **1997**, *36* (40), 12242–51.
- (16) Henderson, I. M.; Bugg, T. D. *Biochemistry* **1997**, *36* (40), 12252–8.
- (17) Lack, N. A.; Yam, K. C.; Lowe, E. D.; Horsman, G. P.; Owen, R. L.; Sim, E.; Eltis, L. D. *J. Biol. Chem.* **2010**, *285* (1), 434–43.
- (18) Fleming, S. M.; Robertson, T. A.; Langley, G. J.; Bugg, T. D. *Biochemistry* **2000**, *39* (6), 1522–31.
- (19) Li, J. J.; Li, C.; Blidauer, C. A.; Bugg, T. D. *Biochemistry* **2006**, *45* (41), 12461–9.
- (20) Pollard, J. R.; Henderson, I. M.; Bugg, T. D. *Chem. Commun.* **1997**, 1185–1186.
- (21) Bhowmik, S.; Horsman, G. P.; Bolin, J. T.; Eltis, L. D. *J. Biol. Chem.* **2007**, *282* (50), 36377–85.
- (22) Li, C.; Montgomery, M. G.; Mohammed, F.; Li, J. J.; Wood, S. P.; Bugg, T. D. *J. Mol. Biol.* **2005**, *346* (1), 241–51.
- (23) Hyland, L. J.; Tomaszek, T. A. J.; Roberts, G. D.; Carr, S. A.; Magaard, V. W.; Bryan, H. L.; Fakhoury, S. A.; Moore, M. L.; Minnich, M. D.; Culp, J. S.; DesJarlais, R. L.; Meek, T. D. *Biochemistry* **1991**, *30* (34), 8441–53.
- (24) Sprinson, D. B.; Rittenberg, D. *Nature* **1951**, *167*, 484.
- (25) Bender, M. L.; Kemp, K. C. *J. Am. Chem. Soc.* **1957**, *79* (116), 116–20.
- (26) Blow, D. M.; Birktoft, J. J.; Hartley, B. S. *Nature* **1969**, *221* (5178), 337–40.
- (27) Hedstrom, L. *Chem. Rev.* **2002**, *102* (12), 4501–24.
- (28) D'Ordine, R. L.; Tonge, P. J.; Carey, P. R.; Anderson, V. E. *Biochemistry* **1994**, *33* (42), 12635–43.
- (29) Schloss, J. V.; Hixon, M. S.; Enol chemistry and enzymology. In *Comprehensive Biological Catalysis*; Academic Press: London, 1997; Vol. 2.
- (30) Begley, T. P.; Ealick, S. E. *Curr. Opin. Chem. Biol.* **2004**, *8* (5), 508–15.
- (31) Buncel, E.; Menon, B. *J. Org. Chem.* **1979**, *44* (3), 317–320.

- (32) Nijvipakul, S.; Ballou, D. P.; Chaiyen, P. *Biochemistry* **2010**, *49* (43), 9241–8.
- (33) Seah, S. Y.; Labbe, G.; Nerding, S.; Johnson, M. R.; Snieckus, V.; Eltis, L. D. *J. Biol. Chem.* **2000**, *275* (21), 15701–8.
- (34) Otwinowski, Z.; Minor, W.; Processing of X-ray diffraction data collected in oscillation mode; *Methods in Enzymology*; Academic Press: New York, 1997; Vol. 276, p 307–326.
- (35) Collaborative Computational Project, Number 4, *Acta Crystallogr., Sect. D: Biol. Crystallogr.* **1994**, *50* (Pt. 5), 760–3.
- (36) Emsley, P.; Cowtan, K. *Acta Crystallogr., Sect. D: Biol. Crystallogr.* **2004**, *60* (Pt. 12 Pt. 1), 2126–32.
- (37) Krissinel, E.; Henrick, K. *Acta Crystallogr., Sect. D: Biol. Crystallogr.* **2004**, *60* (Pt. 12 Pt. 1), 2256–68.
- (38) Chan, Q. W.; Howes, C. G.; Foster, L. J. *Mol. Cell. Proteomics* **2006**, *5* (12), 2252–62.

SUPPORTING INFORMATION

Identification of an acyl-enzyme intermediate in a *meta*-cleavage product hydrolase reveals the versatility of the catalytic triad

Antonio C. Ruzzini^{†‡}, Subhangi Ghosh^{§‡}, Geoff P. Horsman[‡], Leonard J. Foster[†], Jeffrey T. Bolin^{*§}, Lindsay D. Eltis^{*†‡||}.

[†] Department of Biochemistry and Molecular Biology, University of British Columbia, BC, Canada

[§] Purdue Cancer Research Center and Markey Center for Structural Biology, Department of Biological Sciences, Purdue University, West Lafayette, IN, USA

^{||} Department of Microbiology and Immunology, University of British Columbia, BC, Canada

Present address

[‡] Department of Chemistry, Wilfrid Laurier University, Waterloo, Ontario, Canada

Author Contributions

[‡] These authors contributed equally to this work.

Corresponding authors

Jeffrey T Bolin – jtb@purdue.edu

Lindsay D Eltis – leltis@mail.ubc.ca

Table of Contents

Experimental Section

Analysis of steady-state kinetic data S2

Results

Table S1. Properties of the crystals, diffraction data, and refinement statistics S2

Table S2. Results of restrained refinements of ES complexes assuming different isomers of HOPDA S3

Figure S1. BphD H265Q:HOPDA²⁻ protomer and secondary HOPDA²⁻ binding site S3

Figure S2. Whole protein LC ESI/MS analysis of BphD WT and H265Q reacted with excess HOPDA S4

Table S3. *b*-series ion fragment matching results from MASCOT search S5

Figure S3. Representative EI/GC/MS analysis of benzoate, HOPDA, and BphD-catalyzed reactions in H₂¹⁸O S6

Table S4. Example of modeling EI/GC/MS data to ¹⁸O incorporation: WT + HOPDA reaction S7

Table S5. Relative abundance of benzoate and HOPDA ion fragments as analyzed by EI GC/MS S8

Figure S4. Representative stopped-flow experiments monitoring turnover of HOPDA by BphD H265Q S9

Table S6. Kinetic binding data of S112A variants mixed in 2:1 molar excess to HOPDA S10

Figure S5. S112A/H265Q:HOPDA²⁻ complex and representative binding kinetics S11

Figure S6. Representative pre-steady state burst of HPD formation during turnover by BphD WT S12

Table S7 Estimated transition state stabilization by the binding energy of MCP hydrolase side chains S12

Figure S7. Comparison of the acetylated-DAC-AT:substrate complex and the benzoylated BphD H265Q S13

EXPERIMENTAL SECTION

Analysis of steady-state kinetic data. Contributions of individual residues to transition state stabilization were estimated from previously measured steady-state kinetic parameters of BphD and MhpC. The analysis was performed as previously described for a C35G variant of tyrosyl-tRNA synthetase¹. Briefly, the specificity constants were compared using the following equation: $\Delta G_R = RT\ln[(k_{cat}/K_m)_{mut} / (k_{cat}/K_m)_{WT}]$, which assumes that the transition state energy is unaffected by substitution, and that the mutated side-chains do not affect productive binding of a second substrate, in this case H₂O.

RESULTS

Table S1. Properties of the crystals, diffraction data, and refinement statistics

Structure	Crystal properties and diffraction data			
	S112A/H265Q 3V1L	S112A/H265Q:HOPDA 3V1M	H265Q 3V1K	H265Q:HOPDA 3V1N
Crystal growth conditions	2.4 M sodium malonate, pH 6.8	2.4 M sodium malonate, pH 7.0	2.4 M sodium malonate, pH 6.6, 3% v/v ethylene glycol	2.4 M sodium malonate, pH 6.4 10 mM CaCl ₂
Beamline	GM/CA-CAT 23-ID-B	LS-CAT 21-ID-F	GM/CA-CAT 23-ID-D	GM/CA-CAT 23-ID-D
Wavelength (Å)	1.00	0.98	1.00	1.00
Resolution range ^a (Å)	83.1 - 2.1	82.8 - 1.9	117.8 - 2.1	82.5 - 1.6
Space Group	I4 ₁ 22	I4 ₁ 22	P6 ₄	I4 ₁ 22
Cell Dimensions (Å)	<i>a</i> = 117.5, <i>c</i> = 87.8	<i>a</i> = 117.1, <i>c</i> = 87.2	<i>a</i> = <i>b</i> = 135.9, <i>c</i> = 65.8	<i>a</i> = 116.6, <i>c</i> = 87.6
Unique reflections	18,100	23,358	39,208	40,883
Multiplicity ^a	7.6 (3.2)	8.1 (5.0)	10.4 (8.2)	14.0 (11.1)
Completeness ^a (%)	97.8 (91)	99.4 (97)	99.9 (100)	99.9 (99.7)
<i>R</i> _{symm} ^a (%)	12.6 (36.7)	7.5 (38.9)	12.2 (94.8)	7.0 (82.4)
Mean ^a <i>I</i> / <i>σ</i> ²	17.5 (2.7)	24.9 (3.8)	21.0 (2.6)	37.9 (2.8)
Refinement				
<i>R</i> _{factor} / <i>R</i> _{free}	0.18 / 0.22	0.18 / 0.22	0.20 / 0.24	0.18 / 0.21
Model content (atoms)				
Non-hydrogen atoms	2401	2382	4623	2446
Protein ^b	2238	2238	4490	2238
Malonate/HOPDA/benzoyl ^c	7 / 0 / 0	7 / 16 (0.6) / 0	7 / 0 / 0	7 / 16 (0.7) / 8
Water oxygens	156	116	126	177
Average <i>B</i> factors (Å ²)				
all atoms	23.9	25.7	42.0	22.0
protein ^b	23.4	25.5	28.6 ^A / 56.0 ^B	21.4
malonate/HOPDA/benzoyl	27.4 / NA / NA	29.4 / 35.0 / NA	42.9 / NA / NA	25.2 / 28.1 / 21.6
waters	30.5	32.0	43.5	30.0
rmsd ^e bond lengths (Å)	0.01	0.01	0.01	0.01
rmsd bond angles (degrees)	1.3	1.2	1.2	1.4

a – Values for highest resolution bin in parentheses, *b* – All chains include residues 4 - 286 except chain A of H265Q, which includes residues 2 - 286. Atoms modeled in two conformations are counted once. *c* – Each ligand was modeled at full occupancy unless otherwise stated in parentheses; one molecule of malonate = 7 atoms, HOPDA = 16 atoms, benzoyl group = 8 atoms. *d* – For the H265Q structure, values for distinct monomers A and B are indicated by superscripts. *e* – rmsd = root-mean-square deviation from restraint targets

Table S2. Results of restrained refinements of ES complexes assuming different isomers of HOPDA^a

Bond Properties	HOPDA isomer ^{b,c}						
	(2E,4E)-2-hydroxy-6-oxo-(2-enol)	(3E)-2,6-dioxo-(2-keto)	(3E,5Z)-2-oxo-6-oxido-				
Variant	S112A/H265Q	H265Q	S112A/H265Q	H265Q	S112A/H265Q	H265Q	
C1-C2	Initial	-136	53	-171	52	-171	52
	T-refined	-171	53				
	TP-refined	-149	57	-145	61	-146	63
C2-C3	Initial	-4	-166		-165		-165
	T-refined	64	-165	64		64	
	TP-refined	-2	-166	5	-144	-6	-126
C3-C4	Initial	-170	176	171	175	171	175
	T-refined	171	175				
	TP-refined	-173	149	-180	169	-177	171
C4-C5	Initial	177	-109	134	-110	134	-110
	T-refined	134	-110				
	TP-refined	179	-175	161	-131	175	-152
C5-C6	Initial	168	-175	162	-173	162	-173
	T-refined	162	-173				
	TP-refined	171	-142	178	-179	180	177
C6-CB1	Initial	146	173	149	173	149	173
	T-refined	149	173				
	TP-refined	141	-136	146	176	146	-180

a – Initial is the value of the angle of the model prior to any refinement. T-refined is the value after tightly restrained torsion angle refinement. TP-refined is the value after refinement restraining both torsion and planarity. All angles are reported in degrees. *b* – Historical tautomer nomenclature is written in parentheses. *c* – The (3E,5Z)-2-oxo-6-oxido isomer was built into the final model for structures of both ES complexes.

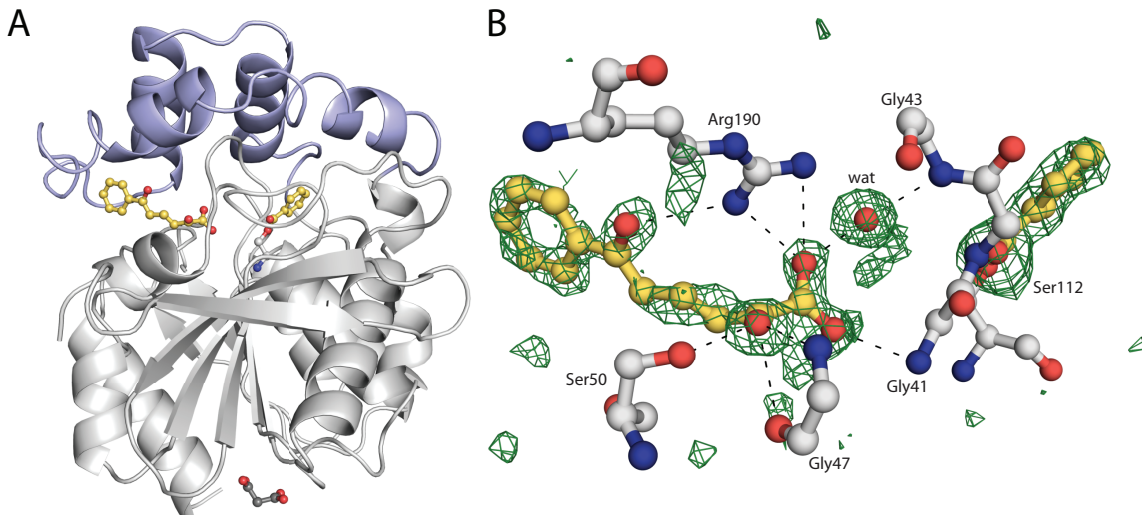


Figure S1. (A) Ribbon drawing of the BphD H265Q structure showing the relative position of the benzoylated active site and secondary HOPDA binding site, located between the core and lid domains. The α/β -hydrolase core (residues 1-145 and 213-286) is colored in white, while the MCP-hydrolase lid domain (residues 146-212) is colored in light blue. (B) Ball-and-stick representation of the BphD H265Q:HOPDA²⁻ complex showing the secondary HOPDA binding site with unbiased F₀-F_c map (green) for HOPDA²⁻, contoured at 3 σ . Putative H-bonding interactions between the substrate, polar residues and a water are indicated. For simplicity, non-polar interactions have been omitted; residues involved include Ala46, Asn51, Leu176, Leu186, Trp266 and Trp269.

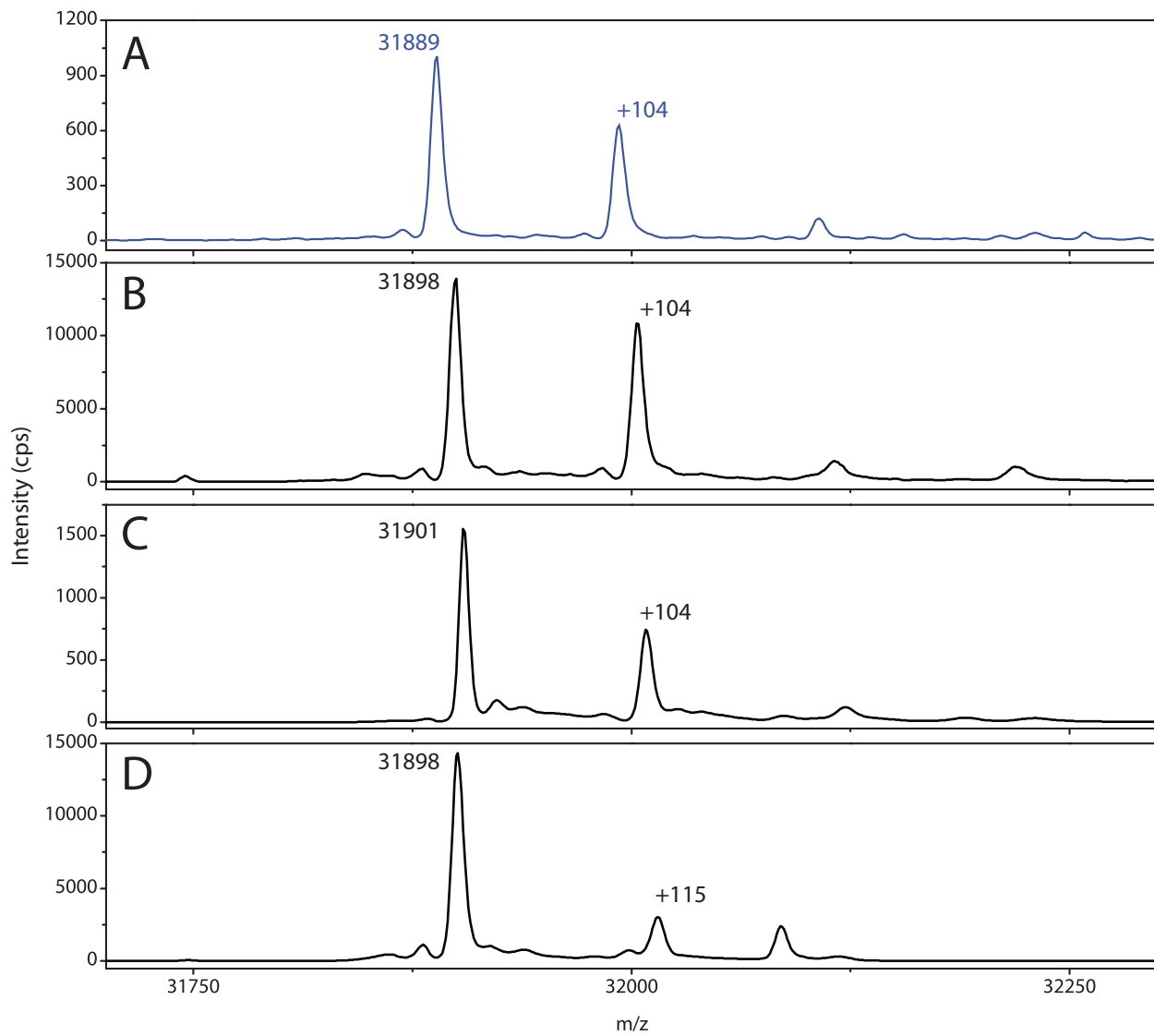


Figure S2. Whole protein LC ESI/MS analysis of H265Q (blue) and WT (black) BphD reacted with HOPDA. Reactions contained 4 μ M enzyme and 20 μ M HOPDA in potassium phosphate ($I = 0.1$ M), pH 7.5 at 25 °C. (A) BphD H265Q-catalyzed reaction quenched after 600 ms. The peak areas indicate that ~40% of the enzyme was acylated. (B) WT-catalyzed reaction quenched after 200 ms. Approximately 45% of the enzyme was acylated. (C) WT-catalyzed reaction quenched after 1 s. Approximately 30% of the enzyme was acylated. The apparent mass shift (+3) was due to the higher noise associated with this dataset. (D) WT-catalyzed reaction quenched after 10 s. No peak corresponding to acylated BphD was detected. The +115 peak is consistent with a non-covalent enzyme:HPD adduct, a reaction product that competitively inhibits BphD.

Table S3. *b*-series ion fragment matches to a BphD peptide analyzed by ESI/MS/MS^{a,b,c}

<i>b</i> -series ion	Peptide		
	WT (unmodified)	WT S112-benzoyl	H265Q S112-benzoyl
<i>b</i> ⁹⁺	977.52 / 977.5163	977.54 / 977.5163	977.51 / 977.5163
<i>b</i> ¹⁰⁺	1091.58 / 1091.5592	1091.58 / 1091.5592	1091.57 / 1091.5592
<i>b</i> ¹¹⁺	1178.61 / 1178.5913		1282.64 / 1282.6175
<i>b</i> ¹²⁺	1309.66 / 1309.6317	1413.69 / 1413.6580	1413.73 / 1413.6580
<i>b</i> ¹³⁺	1366.65 / 1366.6532	1470.69 / 1470.6794	
<i>b</i> ¹⁴⁺	1423.67 / 1423.6747	1527.73 / 1527.7009	
<i>b</i> ¹⁵⁺	1494.74 / 1494.7118	1598.74 / 1598.7380	
<i>b</i> ¹⁷⁺	1666.82 / 1666.7966		
<i>b</i> ^{11*++}	641.83 / 641.8124	589.81 / 589.7993	
<i>b</i> ^{13*++}	735.85 / 735.8434		735.83 / 735.8434
<i>b</i> ^{14*++}	764.36 / 764.3541	712.34 / 712.3410	764.33 / 764.3541
<i>b</i> ^{15*++}	764.85 / 799.8726		
<i>b</i> ^{17*++}	885.97 / 885.9150		
<i>b</i> ^{19*++}	999.95 / 999.4785		
<i>b</i> ^{11*+++}	581.30 / 581.2860		
<i>b</i> ^{16*+++}	789.89 / 789.8701	841.91 / 841.8832	
<i>b</i> ^{17*+++}		877.43 / 877.4018	
<i>b</i> ^{11o+}	1160.61 / 1160.5807		
<i>b</i> ^{16o+}	1577.72 / 1577.7489		
<i>b</i> ^{11o*++}	580.80 / 580.7940		
<i>b</i> ^{16o*++}	789.39 / 789.3781	841.41 / 841.3912	841.37 / 841.3912
<i>b</i> ^{17o*++}		876.91 / 876.9098	876.91 / 876.9098
Search Result Statistics			
Ions score	85	63	50
Expect Value	3.8 E-6	0.00057	0.022
Matches (out of 212)	25	34	23
RMS error (ppm)	207	220	276

a – values of the observed fragments based on manual inspection of raw data and fits to Gaussian peaks followed by MASCOT match results

b – MASCOT search of *B. xenovorans* LB400 proteins resulted in a match to the BphD peptide, DIDRAHLVGNNSMGGATALNF

c – Symbols * and ° indicate ions with an additional loss of NH₃ and H₂O, respectively.

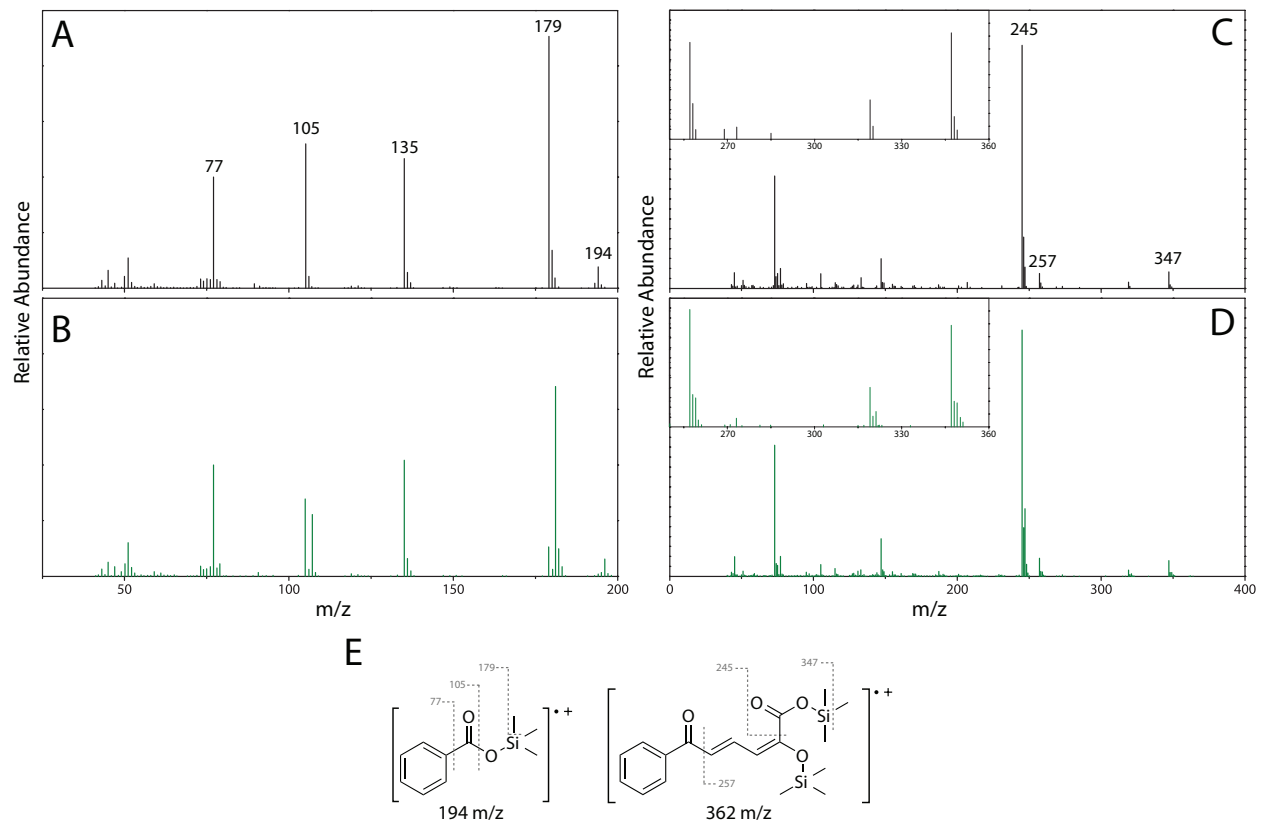


Figure S3. Representative EI/GC/MS analysis of (A) benzoate in H_2O , (B) benzoate derived from BphD-mediated hydrolysis of HOPDA in H_2^{18}O , (C) HOPDA in H_2O , and (D) HOPDA in H_2^{18}O . Inset panels (C and D) highlight the lower intensity HOPDA ion fragments. (E) Illustration of the parent ions and notable fragments.

Table S4. Example of modeling EI/GC/MS data to ^{18}O incorporation: WT + HOPDA reaction

m/z	Observed relative abundance of ions from EI/GC/MS (%)					
	179 [M]	180 [M+1]	181 [M+2]	182 [M+3]	183 [M+4]	184 [M+5]
Control ^a	83.5	12.4	3.9	0.35		
WT + HOPDA ^b	12	2.7	71	10.7	3.6	0.3
Modeling the relative abundance (R.A.) of benzoate species in the sample (%)						
Model 1: Two species accounting for a single ^{18}O incorporation event						
	R.A. [M]	R.A. [M+1]	R.A. [M+2]	R.A. [M+3]	R.A. [M+4]	R.A. [M+5] ^{c,d}
$^{16}\text{O}/^{16}\text{O}$	14	22	16	14		15 ± 1
$^{16}\text{O}/^{18}\text{O}$			84	86	92	86
						85 ± 1
Model 2: Three species including 3% of doubly ^{18}O -incorporated benzoate ^e						
$^{16}\text{O}/^{16}\text{O}$	14	22	16	14		15 ± 1
$^{16}\text{O}/^{18}\text{O}$			84	86	28	-21
						82 ± 3

a – Control values represent the average of all benzoate ion fragments observed in H_2O

b – Benzoate derived from HOPDA incubated with WT BphD for 20 minutes without any pre-incubation

c – The relative abundance of each species ($^{16}\text{O}/^{18}\text{O}$ and $^{18}\text{O}/^{18}\text{O}$) was calculated from the observed intensity of each ion (Obs) from the WT reaction and the control (Co) as follows:

$$\text{R.A. } [\text{M}]_{16\text{O}/16\text{O}} = [\text{M}]_{\text{obs}}/[\text{M}]_{\text{Co}}$$

$$\text{R.A. } [\text{M}+1]_{16\text{O}/16\text{O}} = [\text{M}+1]_{\text{obs}}/[\text{M}+1]_{\text{Co}},$$

$$\text{R.A. } [\text{M}+2]_{16\text{O}/16\text{O}} = ([\text{M}]_{\text{Co}} - [\text{M}+2]_{\text{obs}})/([\text{M}]_{\text{Co}} - [\text{M}+2]_{\text{Co}})$$

$$\text{R.A. } [\text{M}+3]_{16\text{O}/16\text{O}} = ([\text{M}+1]_{\text{Co}} - [\text{M}+3]_{\text{obs}})/([\text{M}+1]_{\text{Co}} - [\text{M}+3]_{\text{Co}})$$

$$\text{R.A. } [\text{M}+4]_{16\text{O}/16\text{O}} = ([\text{M}+2]_{\text{Co}} - [\text{M}+4]_{\text{obs}})/([\text{M}+2]_{\text{Co}} - [\text{M}+4]_{\text{Co}})$$

$$\text{R.A. } [\text{M}+5]_{16\text{O}/16\text{O}} = ([\text{M}+3]_{\text{Co}} - [\text{M}+5]_{\text{obs}})/([\text{M}+3]_{\text{Co}} - [\text{M}+5]_{\text{Co}})$$

$$\text{R.A. of } [\text{M}+\text{N}]_{16\text{O}/18\text{O}} = 1 - [\text{M}+\text{N}]_{16\text{O}/16\text{O}}$$

d – The averages and errors were weighted based on fragment ion intensity

e – The calculation in Table S4 used a model in which 3% of the benzoate contains two equivalents of ^{18}O . Ion fragments derived from this species only contribute to the observed signals at M+4 and M+5: no M+6 or M+7 ions were observed.

Table S5. Relative abundance of benzoate and HOPDA ion fragments as analyzed by EI GC/MS

Sample and Incubation time		Relative abundance (%) ^a of benzoate ion fragments (m/z)					¹⁸ O incorporation ^b
		105 [M]	106 [M+1]	107 [M+2]	108 [M+3]	109 [M+4]	
benzoate	300 min	H ₂ O	92 ± 1	7 ± 1	1.0 ± 0.1		
		H ₂ ¹⁸ O	92.2 ± 0.2	6.7 ± 0.1	1.1 ± 0.1		ND
WT +	300 min	H ₂ O	92.3 ± 0.1	6.6 ± 0.2	1.1 ± 0.1		
benzoate		H ₂ ¹⁸ O	91.5 ± 0.7	7.2 ± 0.5	1.3 ± 0.2		ND
WT +	20 min	H ₂ O	92.2 ± 0.4	6.8 ± 0.8	1.0 ± 0.4		
HOPDA		H ₂ ¹⁸ O	53 ± 2	4.9 ± 0.4	39 ± 3	2.7 ± 0.2	42 ± 1%
WT +	5 min PI	H ₂ O	92 ± 2	7 ± 1	1.0 ± 0.3		
HOPDA	20 min rxn	H ₂ ¹⁸ O	52.9 ± 0.3	5.5 ± 0.9	38 ± 1	3.1 ± 0.2	42 ± 2%
WT +	20 min PI	H ₂ O	91 ± 2	8 ± 1	0.9 ± 0.4		
HOPDA	20 min rxn	H ₂ ¹⁸ O	52.5 ± 0.6	4.8 ± 0.3	38.5 ± 0.4	3.8 ± 0.1	43 ± 2%
			179 [M]	180 [M+1]	181 [M+2]	182 [M+3]	183 [M+4]
							184 [M+5]
benzoate	300 min	H ₂ O	83.2 ± 0.6	12.9 ± 0.5	3.4 ± 0.1	0.44 ± 0.08	
		H ₂ ¹⁸ O	83.1 ± 0.5	12.4 ± 0.3	4.1 ± 0.1	0.4 ± 0.2	ND
WT +	300 min	H ₂ O	84.1 ± 0.4	11.9 ± 0.4	3.6 ± 0.1	0.31 ± 0.01	
benzoate		H ₂ ¹⁸ O	83 ± 0.2	12.3 ± 0.1	4.3 ± 0.1	0.4 ± 0.04	ND
WT +	20 min	H ₂ O	84 ± 1	12 ± 1	3.9 ± 0.1	0.3 ± 0.1	
HOPDA		H ₂ ¹⁸ O	12 ± 1	2.7 ± 0.1	71 ± 2	10.7 ± 0.5	3.6 ± 0.1
WT +	5 min PI	H ₂ O	82.7 ± 0.9	12 ± 1	4.4 ± 0.5	0.4 ± 0.1	0.3 ± 0.1
HOPDA	20 min rxn	H ₂ ¹⁸ O	14 ± 3	3.9 ± 0.3	68 ± 2	11 ± 1	0.23 ± 0.01
WT +	20 min PI	H ₂ O	82.7 ± 0.1	12.8 ± 0.4	4.0 ± 0.4	0.33 ± 0.07	0.3 ± 0.2
HOPDA	20 min rxn	H ₂ ¹⁸ O	16.7 ± 0.4	3.3 ± 0.2	65 ± 1	10.0 ± 0.1	0.5 ± 0.2
			193 [M-1]	194 [M]	195 [M+1]	196 [M+2]	197 [M+3]
							198 [M+4]
benzoate	300 min	H ₂ O	15.7 ± 0.1	70.2 ± 0.7	11.2 ± 0.3	3 ± 1	
		H ₂ ¹⁸ O	18 ± 2	65.6 ± 0.4	12.6 ± 0.1	3 ± 1	ND
WT +	300 min	H ₂ O	15.5 ± 0.3	69 ± 1	12 ± 2	4.0 ± 0.7	
benzoate		H ₂ ¹⁸ O	14.3 ± 0.8	69.5 ± 0.3	11.8 ± 0.3	3.9 ± 0.4	0.39 ± 0.06
WT +	20 min	H ₂ O	17 ± 5	66 ± 1	11 ± 2	5 ± 1	
HOPDA		H ₂ ¹⁸ O	3 ± 1	11 ± 4	15 ± 2	57 ± 8	11 ± 2
WT +	5 min PI	H ₂ O	16 ± 2	69 ± 2	11 ± 4	3 ± 5	2.7 ± 0.8
HOPDA	20 min rxn	H ₂ ¹⁸ O	3.0 ± 0.4	15 ± 1	12 ± 2	55 ± 1	11.5 ± 0.8
WT +	20 min PI	H ₂ O	14 ± 3	71 ± 1	10.7 ± 0.1	5 ± 1	3.0 ± 0.9
HOPDA	20 min rxn	H ₂ ¹⁸ O	4 ± 1	10 ± 1	12.5 ± 0.4	59 ± 2	4.4 ± 0.1
							80 ± 10 %
Relative abundance (%) of HOPDA ion fragments (m/z)							
		245 [M]	246 [M+1]	247 [M+2]	248 [M+3]	249 [M+4]	250 [M+5]
HOPDA	20 min	H ₂ O	78 ± 2	16.0 ± 0.2	5 ± 2	0.5 ± 0.2	
		H ₂ ¹⁸ O	65.0 ± 0.1	12.7 ± 0.2	17.9 ± 0.1	3.2 ± 0.1	1.0 ± 0.2
			257 [M]	258 [M+1]	259 [M+2]	260 [M+3]	261 [M+4]
HOPDA	20 min	H ₂ O	71 ± 5	22 ± 5	6.7 ± 0.1		
		H ₂ ¹⁸ O	62.3 ± 0.3	15 ± 3	18 ± 8	3.1 ± 0.1	1.1 ± 0.1
			347 [M]	348 [M+1]	349 [M+2]	350 [M+3]	351 [M+4]
HOPDA	20 min	H ₂ O	73 ± 6	18 ± 2	8 ± 2	1 ± 1	
		H ₂ ¹⁸ O	58 ± 3	17 ± 2	16 ± 2	6.3 ± 0.8	2 ± 1
							17 ± 5%

^a – errors for relative abundance measurements are a standard deviation from two replicates^b – errors for ¹⁸O incorporation represent the root mean square error from fitting the experimentally observed data to a single ¹⁸O incorporation or to a model that accounts for 2% incorporation of a second ¹⁸O equivalent in parentheses^c – overall rms error based on weighted residual plot analysis, where residual = predicted % intensity from model – observed value

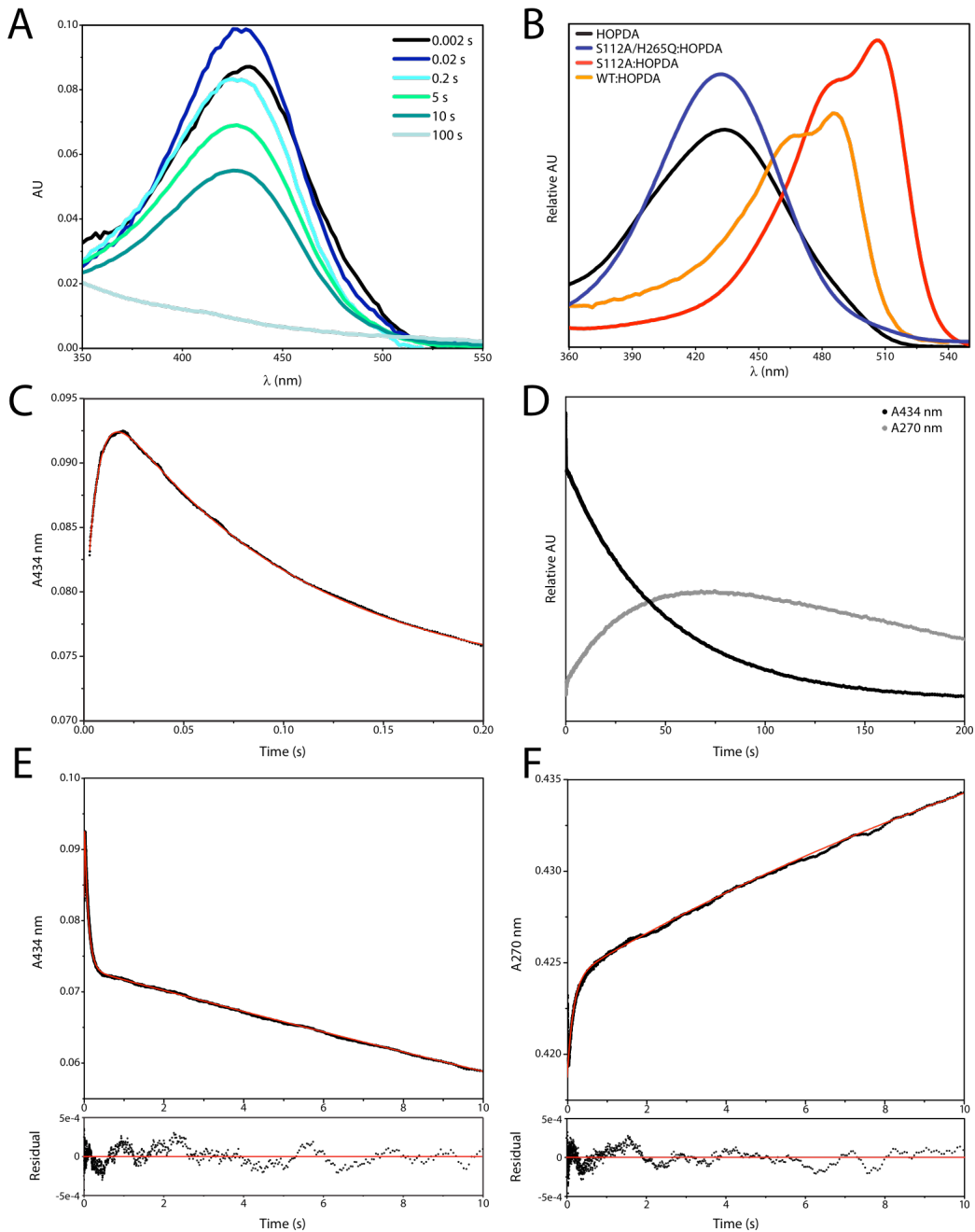


Figure S4. Representative stopped-flow experiments performed in potassium phosphate ($I = 0.1 \text{ M}$), pH 7.5 at 25 °C. (A) Turnover of 4 μM HOPDA by 8 μM BphD H265Q monitored using a photodiode array (note that HOPDAs photodecay under these conditions causing the apparent acceleration of rate constants). (B) The visible absorption spectra of ES complexes in solution. (C) Expanded view of the first 0.2 s during turnover of 4 μM HOPDA by 8 μM BphD H265Q. (D) Turnover of 4 μM HOPDA by 8 μM BphD H265Q monitored for 200 s, the normalized relative $\Delta A_{434} \text{ nm}$ and $\Delta A_{270} \text{ nm}$ are shown in black and grey, respectively, in order to demonstrate the reactions goes to completion under these conditions. (E) Turnover of 4 μM HOPDA by 8 μM BphD H265Q monitored at 434 nm for 10 s. Traces were fit from 0.003 to 10 s with a triple exponential equation (fit in red). The residual is shown below. (F) Turnover of 4 μM HOPDA by 8 μM BphD H265Q monitored at 270 nm for 10 s. Traces were fit from 0.02 to 10 s with a triple exponential equation (fit in red). The residual is shown below.

Table S6. Kinetic binding data of S112A variants mixed in 2:1 molar excess to HOPDA^a

Enzyme	λ (nm)	Formation of ES ^{red} or ES ^{planar}						λ_{\max} (nm)	$t_{1/2}$ (h)
		k_1 (s ⁻¹) [% Amp]	k_2 (s ⁻¹) [% Amp]	k_3 (s ⁻¹) [% Amp]					
S112A ^b	492	~ 500	[85]	76	[11]	0.92	[4]	488 / 506	4.4
S112A/H265A ^b	434	220	[69]	22	[22]	0.34	[9]	432	ND
S112A/H265Q	434	114 ± 8	[39]	32 ± 2	[38]	0.78 ± 0.02	[22]	432	31

a – all rates are associated with increasing absorptivity at the stated wavelength.*b* – data was taken from Horsman *et al* (2007)².

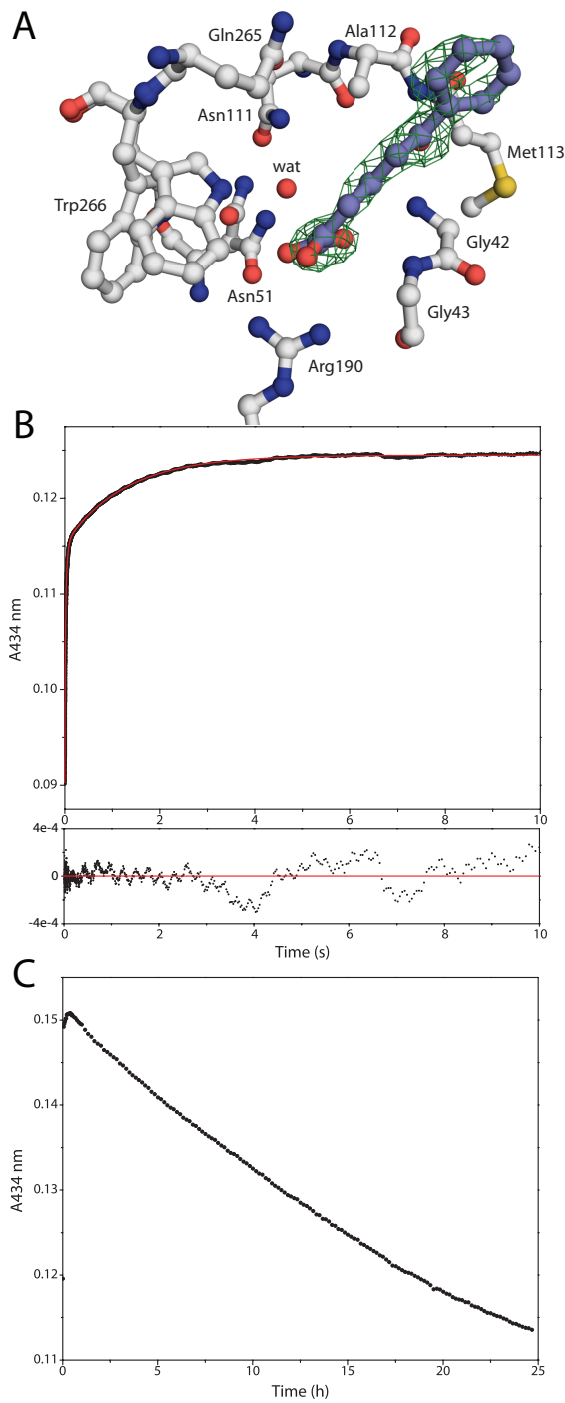


Figure S5. (A) Ball-and-stick representation of the BphD S112A/H265Q:HOPDA²⁻ complex active site, including the unbiased Fo-Fc map (green) for the substrate, contoured at 3σ. Polar contacts are shown using dashed lines. Hydrophobic interactions between the ligand and Ala112, Gly138, Ile153, Leu156, Phe175, Leu213, Trp216, Val240, and Trp 266 have been omitted for simplicity. (B) Representative stopped-flow replicate showing the binding of HOPDA²⁻ to S112A/H265Q in potassium phosphate ($I = 0.1\text{ M}$), pH 7.5 at 25 °C. (C) Representative trace used for estimating the half-life of the S112A/H265Q:HOPDA²⁻ complex.

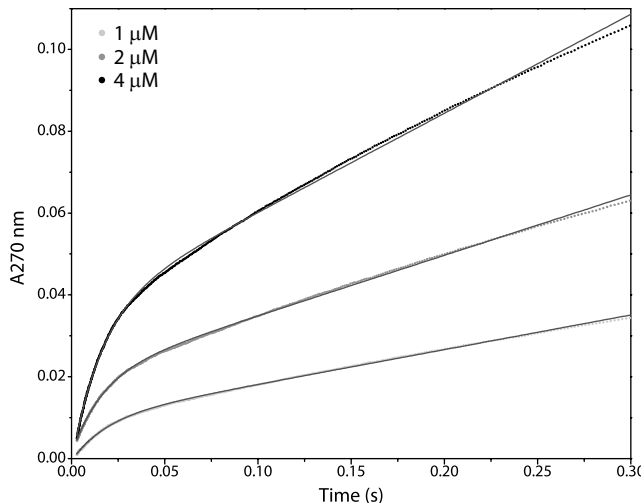


Figure S6. Representative stopped-flow experiments demonstrating a pre-steady state burst of HPD formation by BphD WT in potassium phosphate buffer ($I = 0.1$ M), pH 7.5 at 25 °C. The slight divergence from linearity in the traces can be explained by substrate depletion, which was ~18% after 0.5 s at 4 μ M enzyme. Consequently, product accumulation and inhibition ($K_{ic\text{ HPD}} \sim 80$ μ M, $K_{iu\text{ HPD}} \sim 120$ μ M, $K_{ic\text{ benzoate}} \sim 160$ μ M), and non-enzymatic enolization of HPD, associated with a decay of the signal at 270 nm ($k \sim 0.6$ s⁻¹), likely accounts for the reduction in the apparent steady-state rate with increasing enzyme concentration³.

Table S7. Estimated transition state stabilization by the binding energy of MCP hydrolase side chains to HOPDA.

Enzyme	k_{cat}/K_m (M ⁻¹ s ⁻¹)	$ \Delta G_R $ (kcal mol ⁻¹)	Ref
BphD wild type, pH 7.5	3.2×10^6		⁴
S112C	9.5×10^4	2.1	³
BphD wild-type, pH 8.0	3.3×10^6		⁵
R190Q	5.7×10^2	5.1	⁵
R190K	2.8×10^3	4.2	⁵
MhpC, pH 8.0	4.1×10^6		⁵
N109A	3.3×10^4	2.9	⁵
N109H	1.9×10^4	3.2	⁵
F173G	1.3×10^4	2.0	⁵
F173D	2.6×10^4	3.0	⁵
R188Q	1.4×10^3	4.7	⁵
R188K	1.9×10^4	3.2	⁵
C261A	2.9×10^6	0.2	⁵
W264G	2.1×10^4	3.1	⁵

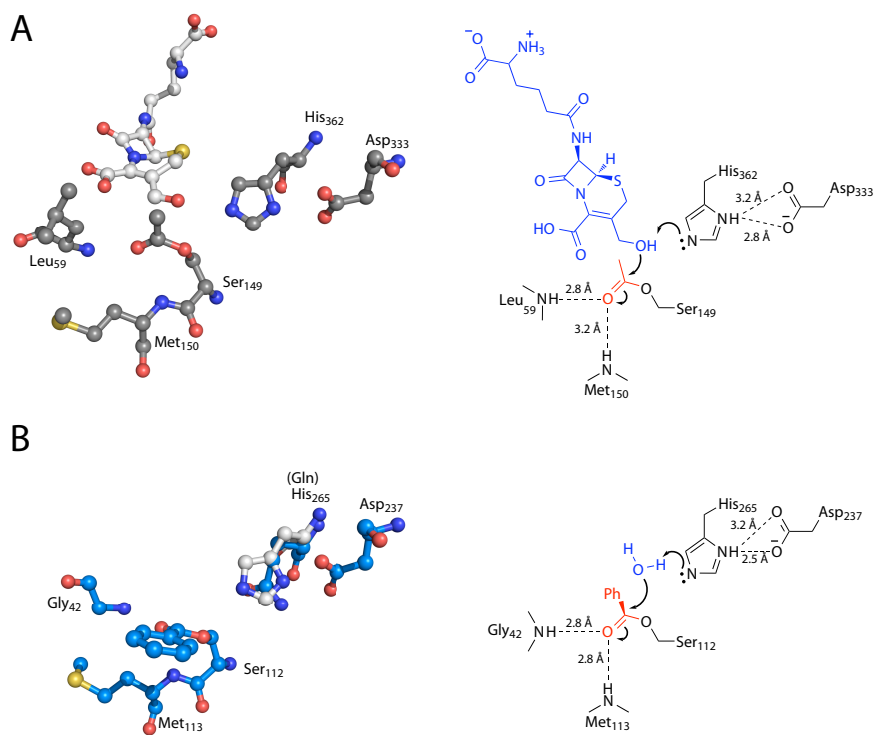


Figure S7. (A) *Left*. Ball-and-stick representation of the acetylated DAC-AT:deacetylcephalosporin C active site (PDB ID: 2VAV Chain L⁶). *Right*. Interpretation of the chemical reaction leading to acetylation by DAC-AT. (B) *Left*. Ball-and-stick representation of the benzoylated BphD H265Q active site, and superposition of His265 from 2OG1 chain B. *Right*. By analogy, the activation of water by the His-Asp dyad is drawn in context of the MCP-hydrolase mechanism.

REFERENCES

1. Wilkinson, A. J.; Fersht, A. R.; Blow, D. M.; Winter, G., *Biochemistry* **1983**, 22 (15), 3581-6.
2. Horsman, G. P.; Bhowmik, S.; Seah, S. Y.; Kumar, P.; Bolin, J. T.; Eltis, L. D., *J Biol Chem* **2007**, 282 (27), 19894-904.
3. Horsman, G. P.; Ke, J.; Dai, S.; Seah, S. Y.; Bolin, J. T.; Eltis, L. D., *Biochemistry* **2006**, 45 (37), 11071-86.
4. Bhowmik, S.; Horsman, G. P.; Bolin, J. T.; Eltis, L. D., *J Biol Chem* **2007**, 282 (50), 36377-85.
5. Li, C.; Li, J. J.; Montgomery, M. G.; Wood, S. P.; Bugg, T. D., *Biochemistry* **2006**, 45 (41), 12470-9.
6. Lejon, S.; Ellis, J.; Valegard, K., *J Mol Biol* **2008**, 377 (3), 935-44.